

# The International Journal of Robotics Research

<http://ijr.sagepub.com>

---

## **Orienting Toleranced Polygonal Parts**

Srinivas Akella and Matthew T. Mason

*The International Journal of Robotics Research* 2000; 19; 1147


DOI: 10.1177/02783640022068002

The online version of this article can be found at:

<http://ijr.sagepub.com/cgi/content/abstract/19/12/1147>

---

Published by:

 SAGE Publications

<http://www.sagepublications.com>

On behalf of:



Multimedia Archives

**Additional services and information for *The International Journal of Robotics Research* can be found at:**

**Email Alerts:** <http://ijr.sagepub.com/cgi/alerts>

**Subscriptions:** <http://ijr.sagepub.com/subscriptions>

**Reprints:** <http://www.sagepub.com/journalsReprints.nav>

**Permissions:** <http://www.sagepub.com/journalsPermissions.nav>

**Citations** (this article cites 13 articles hosted on the  
SAGE Journals Online and HighWire Press platforms):  
<http://ijr.sagepub.com/cgi/content/refs/19/12/1147>

---

## Srinivas Akella

Department of Computer Science  
Rensselaer Polytechnic Institute  
Troy, New York 12180, USA  
sakella@cs.rpi.edu

## Matthew T. Mason

School of Computer Science  
Carnegie Mellon University  
Pittsburgh, Pennsylvania 15213, USA

# Orienting Toleranced Polygonal Parts

## Abstract

*Parts manufactured to tolerances have variations in shape. Most previous work in robotic manipulation assumes that parts do not have shape variations. Orienting devices such as bowl feeders often fail due to variations in part shape. We study the effects of uncertainty in part shape on orienting to develop systems that can orient toleranced polygonal parts. We present a tolerance model in which the part center of mass and vertices lie in circular uncertainty zones around their nominal positions. The variations in part shape are characterized by the tolerance model and the part's nominal shape. We describe the nondeterminism that arises due to part shape uncertainty for a conveyor-based orienting system and show that sensor-based and sensorless orienting plans can exist for toleranced polygonal parts. We present implemented planners that generate orienting plans for the entire variational class of part shapes given a nominal part shape and tolerance bounds. These plans use both deterministic and nondeterministic actions to orient the parts, and we describe experiments to demonstrate them.*

**KEY WORDS**—parts orienting, tolerancing, flexible assembly, manufacturing

## 1. Introduction

Parts manufactured to tolerances have variations in shape. Most previous work in robotic manipulation assumes that the part shape is known exactly and that parts have no shape variations. Orienting devices such as bowl feeders frequently fail due to variations in part shape, particularly when parts are supplied by multiple manufacturers. Consequently, it is important to develop systems that can orient toleranced parts. We characterize the effects of uncertainty in part shape on the

orienting process for a conveyor-based parts-orienting system and identify conditions under which we can generate orienting plans for toleranced polygonal parts. We present a tolerance model in which the part center of mass and vertices lie in circular uncertainty zones around their nominal positions. The *variational class* (Requicha 1983) of parts for a given nominal part shape and tolerance model is the class of all part shapes that satisfy the tolerance bounds. Given a nominal part shape and tolerance bounds, we generate orienting plans for the variational class of part shapes.

Part shape critically influences the orientability of parts, as illustrated by Goldberg (1993) and Caine (1994). Rao and Goldberg (1994) and Akella and Mason (1999) have described planning algorithms to orient a single part shape and a finite set of known part shapes and have shown that every polygonal part has a corresponding infinite set of part shapes with identical mechanical behavior. Orienting a toleranced part, however, involves generating a plan for an infinite set of part shapes that are valid instances of the given variational class and that do not have identical mechanical behavior. We address the issue of generating orienting plans for toleranced polygonal parts in this paper and present the following results:

1. Uncertainty in the shape of a toleranced part introduces nondeterminism in the parts-orienting process.
2. We show that both sensor-based and sensorless plans to orient toleranced polygonal parts exist.
3. We have implemented planners and demonstrated parts orienting in the presence of shape uncertainty.

The paper is organized as follows. After an outline of related work in Section 2, Section 3 reviews our prior work (Akella and Mason 1999) on orienting parts with known shape using partial information sensors. Section 4 then presents our tolerance model and Section 5 describes the nondeterminism

in parts orienting that arises from shape uncertainty. Section 6 presents algorithms to classify each part edge as stable, unstable, or sometimes-stable for the input tolerance values. Section 7 focuses on computing actions for the class of polygonal parts with a constant set of stable edges, and Sections 8 and 9 show that sensor-based and sensorless orienting plans can exist even with shape uncertainty. Section 10 characterizes completeness properties of these planners, and Section 11 outlines a planner for parts whose set of stable edges may change due to shape uncertainty. Section 12 describes implemented planners that generate sensor-based and sensorless plans for the class of parts with a constant set of stable edges. Section 13 concludes with a discussion of future work.

## 2. Related Work

The need to manufacture parts specified by tolerances arose with the development of mass production methods that required parts that could work interchangeably (Voelcker 1993). Current industrial standards include the ASME Y14.5M-1994 tolerancing and dimensioning standard (American Society of Mechanical Engineers 1995).

Requicha (1983, 1984) developed a mathematical formalism for the analysis and design of toleranced parts. He used tolerance zones to describe the valid variational class of parts and offset operations to generate these tolerance zones. Requicha (1993) surveys various approaches to tolerancing and uses the offset zone tolerancing technique to describe the advantages of a mathematical theory of tolerances. Voelcker (1993) surveys the area of tolerancing and describes the trend toward tolerancing standards chosen on a mathematical basis over those specified by figures and examples. The goals are to avoid ambiguous interpretations, establish correct measurement techniques, and identify data structures and algorithms suitable for use in geometric modeling systems. Neumann (1994) describes the new dimensioning and tolerancing standard, ASME Y14.5M, and Walker and Srinivasan (1994) describe a companion standard, ASME Y14.5.1M-199X, that provides a mathematical basis for dimensioning and tolerancing. Yap (1995) advocates using computational geometry and exact computation techniques to develop algorithms for tolerancing metrology, for tasks such as estimating the deviations from tolerance of manufactured parts using a set of sampled measurements.

Probably the earliest work that explicitly considered geometric shape uncertainty for a manipulation problem was by Donald (1989, 1990). He defined a generalized configuration space with additional dimensions for the parametric variations in the part features and used it to generate multiple-step compliant motion error detection and recovery (EDR) strategies. Brost (personal communication, August 1994) developed a tolerance model and has used it (Brost and Peters 1996) in

the automatic design of fixtures that are robust to variations in part shape. Brost's model specifies tolerance zones by choosing an uncertainty polygon for each vertex and sweeping it along the two polygon edges adjacent to the vertex. Latombe, Wilson, and Cazals (1997) studied the problem of assembly sequencing with toleranced parts. They present an algorithm to determine if an assembly sequence exists for all instances of the components within the specified tolerances, and to generate it when it exists. They assume part edges vary only in position and not in orientation, and focus on the geometric clearance issues for assembly without considering assembly stability. Joskowicz, Sacks, and Srinivasan (1997) compute the variations in kinematic behavior of mechanisms from the tolerance specifications of their parts. They present a kinematic tolerance space that encodes the quantitative and qualitative effects of part variations on kinematic function. Inui, Miura, and Kimura (1996) analyze the variations in relative positions of two contacting parts when there are variations in their shapes. Deacon, Wright, and Malcolm (1997) consider the effect of changing the center of mass location on the stability of a robot pushing operation. Kavraki (1997) proposes a vector field designed to bring most parts to two stable equilibria and characterizes the variation in equilibrium orientations for toleranced parts.

Our work was previously reported in Akella (1996) and Akella and Mason (1998). It relies on previous results on the mechanics and planning of pushing and grasping operations (Mason 1986; Brost 1988; Peshkin and Sanderson 1988; Goldberg 1993). It is also related to sensor-based manipulation planning using AND/OR search (Taylor, Mason, and Goldberg 1988) and sensor-based orienting of multiple parts by parallel-jaw grasping (Rao and Goldberg 1994). The tolerance model we use here is a parametric model that permits variations in both the orientations and positions of part edges (Akella and Mason 1995). Akella and Mason (1999) used partial information sensors with manipulation operations to orient and recognize parts. They describe a form of shape uncertainty where an infinite set of polygonal parts behave identically when pushed; any member of the set can therefore be oriented by the same plan.

The work most closely related to ours is that of Chen et al. (1998) on sensorless orienting and fixturing of toleranced parts. For orienting, they use a tolerance model similar to ours, where part instantiations belong to the tolerance class if their vertices lie within the vertex uncertainty disks when the instantiated and nominal centers of mass are made to coincide. Since not all parts consistent with the vertex uncertainty regions are included in the tolerance class, the variational class of parts under their model is a subset of the variational class under our model. They compute approximate bounds on the maximum radius of the vertex uncertainty disks for which a plan exists and modify Chen and Ierardi's (1995) algorithm to generate sensorless orienting plans. They also analyze

fixturing with a right-angle fixel and a clamp for a tolerance model where the vertices are assumed to lie in a square centered at the nominal vertex.

### 3. Orienting a Known Part Shape

We build on our previous work on orienting parts with known shape using partial information sensors (Akella 1996; Akella and Mason 1999). We assume a part in an unknown initial orientation drifts on a conveyor belt until it contacts a fence placed perpendicular to the motion direction (Fig. 1). The part rotates against the fence until one of its stable edges aligns with the fence. An LED sensor measures the resting diameter, or width, of the part perpendicular to the fence to obtain partial information on the part orientation. An orienting plan is a sequence of *push-align operations* the robot executes to orient the part. Each operation consists of an action followed by a sensor measurement of the diameter of the aligned part. The action consists of the robot picking up an aligned part at the fence using a suction cup, translating upstream from the fence, rotating the part through a chosen angle, and then releasing the part on the conveyor for it to be aligned at the fence. We define *orienting a part* to mean identifying the part edge that is aligned against the fence.

We make the following assumptions in analyzing this orienting system:

1. All parts are polygonal.
2. All motions are in the plane and are quasi-static.
3. The fence is normal to the conveyor motion direction.
4. All frictional interactions are described by Coulomb friction.
5. The coefficient of friction between the part and the conveyor surface is uniform.
6. All bodies in contact are perfectly rigid.

When a part on the moving conveyor contacts the stationary fence, it is pushed normal to the fence face. Viewed from a frame fixed in the belt, this is a *linear normal push*, where a moving fence pushes a part in a direction normal to the fence face. The part rotation due to such a push can be predicted using the *radius function* (Goldberg 1993). The radius function of a polygon is a mapping from the orientation  $\phi$  of a supporting line of the polygon to the perpendicular distance  $r$  from a reference point in the polygon to the supporting line (Fig. 2). When the center of mass is the reference point and the fence is the supporting line, the local minima of the radius function correspond to stable edges of the part. An edge is *stable* if the projection of the center of mass onto the edge lies in the interior of the edge. An edge is *unstable* if the projection of

the center of mass onto the edge lies outside the edge, and is *metastable* if the center of mass projects onto a vertex of the edge. A *transition vertex* is a vertex at which a maximum of the radius function occurs. A part being pushed against a fence rotates to achieve a minimum radius and comes to rest with one of its stable edges aligned with the fence. Each local minimum determines a convergent orientation and each local maximum determines a divergent orientation. A push has the net effect of mapping the entire interval between two divergent orientations to the enclosed convergent orientation.

The *resting range* of a stable orientation or stable edge of a part is the set of initial part orientations for which the part comes to rest in that stable orientation (Fig. 3). The stable orientations correspond to the minima of the radius function, and the resting range limits are obtained from the enclosing maxima of the stable orientations on the radius function. Each resting range limit of a stable edge corresponds to the maximum clockwise (counterclockwise) rotation of the part from the edge such that the line joining its counterclockwise (clockwise) transition vertex to the center of mass is perpendicular to the fence.

The *action range* of a stable edge  $e_i$  with respect to a destination stable edge  $e_j$  is the maximal interval of rotations for which the part transitions from edge  $e_i$  to edge  $e_j$ . Each stable edge of a part with  $n$  stable edges has  $n$  action ranges. Consider the range of actions to transition from start state  $s_i$  to destination state  $s_j$ , where state  $s_i$  corresponds to edge  $e_i$  (Fig. 4). Let the stable orientation of state  $s_i$  be  $\psi_i$ , and the right and left limits of the resting range of state  $s_j$  be  $\rho_j$  and  $\lambda_j$ . Any action in the open interval  $(\lambda_j - \psi_i, \rho_j - \psi_i)$  will cause a deterministic transition from  $s_i$  to  $s_j$ . That is, any counterclockwise rotation  $\theta \in (\alpha^{\min}, \alpha^{\max})$ , where  $\alpha^{\min} = \lambda_j - \psi_i$  and  $\alpha^{\max} = \rho_j - \psi_i$ , causes a transition from edge  $e_i$  to edge  $e_j$ . Thus, the action ranges for the transitions from  $s_i$  to every other state, and between every pair of states, are computed from the resting ranges.

The action ranges for a given set of states (i.e., edges) are determined from the action ranges of the individual states. The set of intervals corresponding to the action ranges from the individual states are overlapped to obtain another set of intervals, the *overlap ranges*. For the given set of initial states, any action from an overlap range gives the same resulting set of states. A representative action is selected from the middle of each overlap range, and these actions are used to generate orienting plans.

We have shown (Akella and Mason 1999), for parts with known shape, that sensor-based and sensorless plans exist to orient polygonal parts up to symmetry, and have implemented planners to generate such plans. Sensor-based plans distinguish states by their diameter values. The sensor-based plan length is typically bounded by  $m$  operations and is never greater than  $2m - 1$  operations, where  $m$  is the maximum number of states with indistinguishable diameter values.

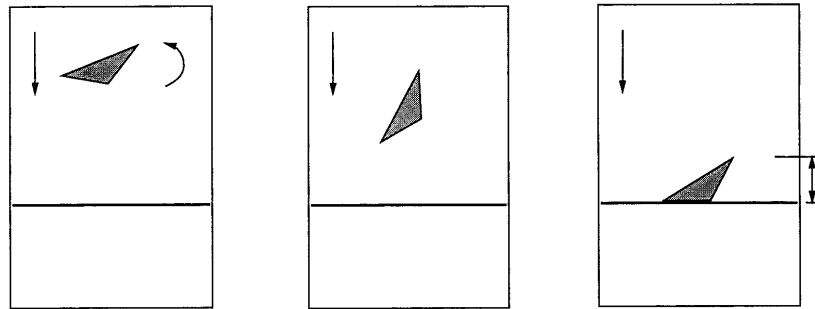


Fig. 1. Schematic overhead view of a part on the conveyor during a push-align operation, shown from left to right. The conveyor motion is "downward." The robot first picks up a part and rotates it through a chosen angle before placing it on the conveyor. The part then drifts on the conveyor into contact with the fence. The part rotates into alignment with the fence and its diameter is then sensed.

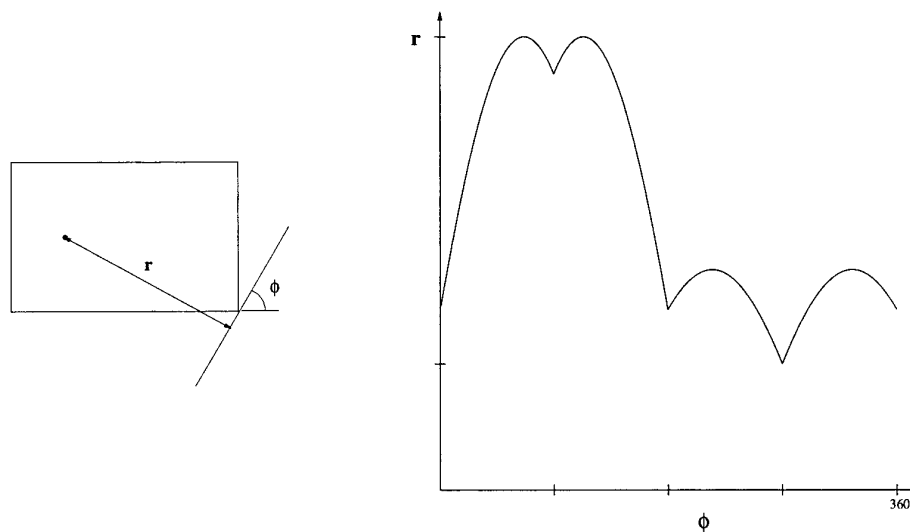


Fig. 2. The radius function for the rectangle, with its center of mass indicated by the black dot. The radius  $r$  of a part at a fence orientation  $\phi$  is the perpendicular distance from the center of mass to the fence. The radius function is the plot of the part radius as the fence orientation is varied, and wraps around at 360 deg. Based on Goldberg (1993).

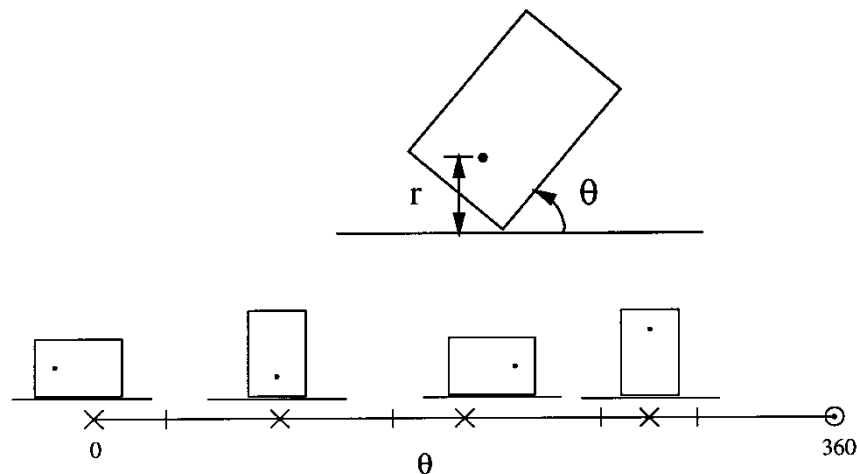


Fig. 3. Resting ranges for the rectangle of Figure 2. The x's indicate stable orientations of the rectangle for each resting range, and the vertical bars indicate the limits of each resting range. This diagram corresponds to a slice of the push stability diagram of Brost (1988) along the 90-deg pushing direction.

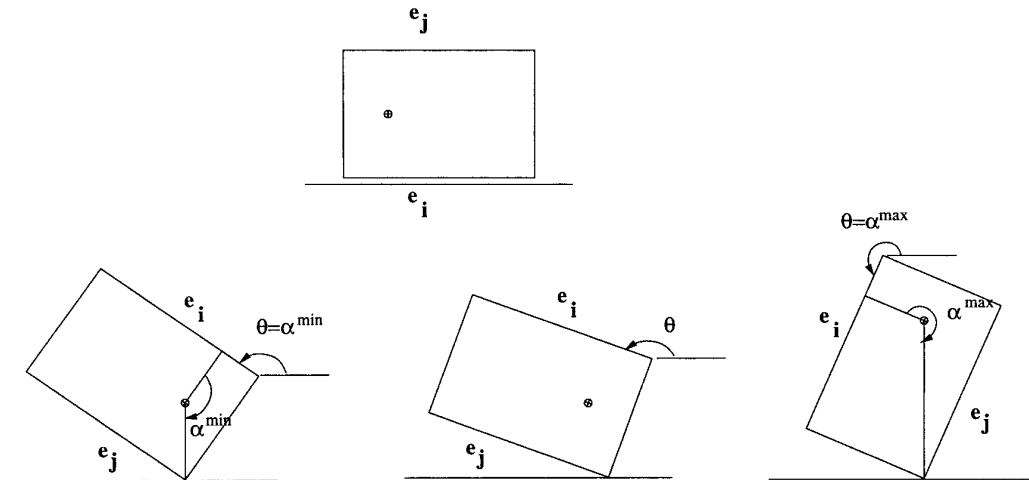


Fig. 4. The rectangle transitions from edge  $e_i$  to edge  $e_j$  for any  $\theta \in (\alpha^{\min}, \alpha^{\max})$ , when its exact shape is known.

#### 4. The Tolerance Model

The tolerance model we present can be viewed as a parametric model that permits variations in both the orientations and positions of part edges. We make the following assumptions in modeling the uncertainty in the shape of a polygonal part (Fig. 5):

- The nominal shape of the part, defined by the positions of its vertices and center of mass, is known.
- We consider only convex polygons that remain convex for all instantiations of the tolerance values. That is, every member of the variational class is a convex polygon.
- Each vertex lies inside a circular disk of radius  $r_v$  centered at its nominal location. This radius is a specified input variable.
- The center of mass lies inside a circular disk of radius  $r_c$  centered at its nominal location. This radius can be computed as a function of  $r_v$  and the polygon shape, or can be specified as an independent input variable.
- The vertex uncertainty disks do not intersect each other and do not intersect the center of mass uncertainty disk. The uncertainty disk at each vertex intersects only the two edges incident at that vertex.
- The actual part edges are straight lines connecting the actual vertex positions.

Any part that lies within the class of shapes defined by the nominal shape and the tolerance model belongs to the variational class of parts we wish to orient. Note that the center of mass location and its uncertainty disk radius can be specified independent of the vertex locations and uncertainty

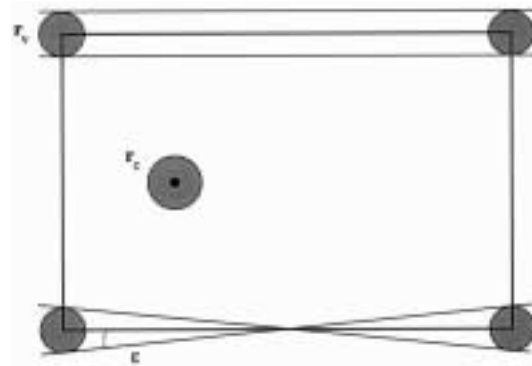


Fig. 5. Tolerance model showing the center of mass and vertex uncertainty disks. The nominal center of mass and polygon edges are drawn bold. The extremal positions and orientations of the longest edges are also indicated.

radii. We do not consider polygonal parts that do not satisfy the above assumptions, such as those in Figure 6.

##### 4.1. Selecting a Tolerance Model

Our tolerance model is motivated by the need to characterize the range of orientations from which a part may rotate to a given stable edge. This depends on the relative positions of the center of mass and the transition vertices for the edge. Since the vertex and center of mass uncertainty regions are explicitly bounded, we can compute these orientation ranges for toleranced parts. The similar model of Chen et al. (1998) is simpler in that it corresponds to having a zero radius center of mass uncertainty disk and does not permit the center of mass position to vary independently of the vertex positions. Alternative tolerance models have been developed for other tasks, including those of Requicha (1983), Brost (personal communication, August 1994), and Latombe, Wilson, and Cazals (1997). Requicha's model specifies tolerance zones



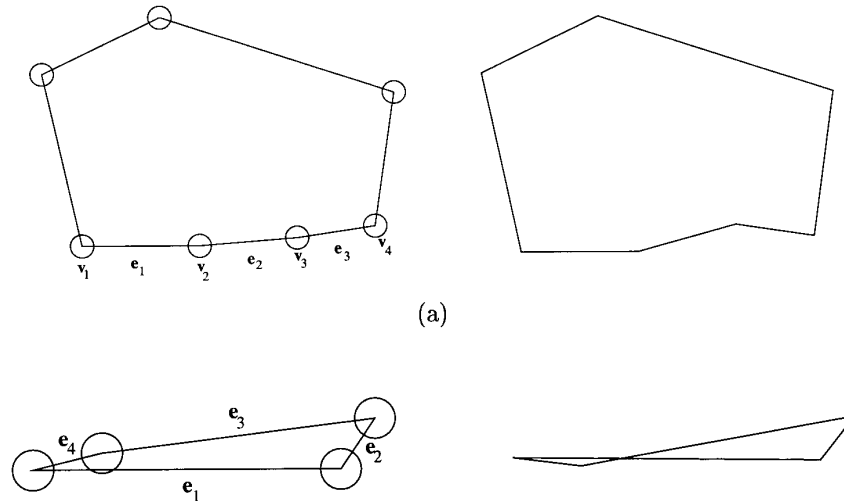


Fig. 6. These parts do not satisfy the assumptions of our model. (a) The part has three adjacent edges,  $e_1$ ,  $e_2$ , and  $e_3$ , that are almost parallel. The vertices  $v_2$  and  $v_3$  can become concave. This is shown for vertex  $v_3$  at right. (b) Edges  $e_3$  and  $e_4$  of the quadrilateral can cross edge  $e_1$ , as shown at right.

by sweeping out circles of specified radii along the polygon edges. Brost's model specifies tolerance zones by choosing an uncertainty polygon for each vertex and sweeping it along the two polygon edges that meet at the vertex. The models of Requicha and Brost place no restrictions on the shapes of the edges and permit the vertices to lie outside their uncertainty regions provided the edges lie inside their tolerance zones. Latombe, Wilson, and Cazals's model specifies tolerance zones by sweeping each edge of the polygon through a specified positional range, with no variations in edge orientation. Each vertex is restricted to a corresponding parallelogram region. Any such shape uncertainty model in which the center of mass and vertex uncertainty regions are explicitly bounded can be handled by our method.

Our model enables us to quantify variations in action ranges and edge orientations in terms of the tolerance parameters, independent of the manufacturing process. This work represents a first step toward our long-term goal of developing tolerance models that lend themselves to such analysis while incorporating true shape variations arising from manufacturing processes.

## 5. Effects of Shape Uncertainty

Shape uncertainty under our tolerance model causes the following variations:

1. *Variations in orientations of part edges:* Variations in edge orientations can be computed directly from the tolerance values. For a vertex uncertainty disk radius  $r_v$ , the maximum and minimum orientations of an edge of nominal length  $l$  are computed from the common tangents to the vertex uncertainty disks at the nomi-

nal vertex positions. The edge orientation lies between  $\psi - \epsilon$  and  $\psi + \epsilon$ , where  $\psi$  is the nominal edge orientation and  $\epsilon = \sin^{-1}(2r_v/l)$ .

2. *Variations in the diameter values at the stable orientations:* The diameter of the part normal to the fence when aligned against it can vary from the nominal size by  $2r_v$  (Fig. 5). For a nominal diameter value of  $d$ , the actual diameter lies in the interval  $[d - 2r_v, d + 2r_v]$ .
3. *Variations in the center of mass location:* The center of mass depends on the part shape. Computing the exact center of mass (COM) uncertainty locus for a given tolerance bound is an open problem. We model the variation in the center of mass with a disk of radius  $r_c$ , centered at the nominal COM, that bounds the locus of possible center mass locations. See the appendix for details.
4. *Variations in the resting and action ranges of the edges:* Uncertainty in the positions of the vertices and the center of mass causes variations in the resting ranges. The uncertainty in the limits of the resting ranges can be determined from the angles defined by the common tangents to the center of mass uncertainty disk and the uncertainty disks for the clockwise (CW) and counter-clockwise (CCW) transition vertices of the edge. The action ranges can be obtained from the resting ranges as described in Section 7.
5. *Variations in the set of stable edges:* The set of stable edges for a given instantiation of the part depends on the center of mass location and the edge positions and orientations. Identifying all possible combinations of

stable edges that can occur requires an analysis of edges that can be stable. We defer a more detailed discussion to Section 6.

### 5.1. Nondeterminism

The main operational effect of shape uncertainty on parts orienting is to introduce nondeterminism, which comes from variations in the outcomes of actions and variations in the set of stable edges.

The actions for a particular instantiation of a part shape are deterministic. Over the variational class of parts, however, some of the actions are effectively nondeterministic actions. Consider the two instantiations of the part shown in Figure 7 (b) and (c). A push-align action that brings the two instantiations to the same initial orientation results in a CCW rotation for the first instantiation and a CW rotation for the second instantiation. The action is deterministic for each instantiation, but since it has different outcomes for the two, we must treat it as a nondeterministic action. Actions that lead to different outcomes for different part instantiations must be treated as nondeterministic actions over the variational class of part shapes.

The set of stable edges for a particular instantiation of a part shape is constant. Over the variational class of parts, the center of mass position relative to each edge varies, and the set of stable edges may therefore change. Edges of a part that are stable in its nominal shape may become unstable for some instantiations of the part, or unstable edges of the part may become stable (Fig. 8). These variations in the set of stable edges also manifest themselves as nondeterministic behavior.

These nondeterministic effects complicate the orienting task. We first tackle the problem of planning with shape uncertainty when the set of stable edges does not change. While the size, position, and orientation of each stable edge can vary, these edges are always stable for all instances of the variational class, and no other edges become stable. We present implemented planners for polygons with a constant set of stable edges in Section 8 and Section 9, and we outline in Section 11 a planner for polygons whose set of stable edges may change. We begin by identifying in the next section conditions under which the set of stable edges is constant.

## 6. Edge Stability Regions

The set of stable edges depends on the location of the center of mass relative to the edges. To satisfy the assumption that the set of stable edges of the polygon does not change, we must ensure that the center of mass always lies in the appropriate region of the polygon. For a part with known shape, the *stability region* of an edge is the set of center of mass locations for which the edge is stable. It is the set of points in the polygon interior whose perpendicular projections onto the edge lie in its interior. All points between the inward normals to

the edge at its CW and CCW vertices,  $n_{cw}$  and  $n_{ccw}$ , respectively, in the polygon interior constitute the stability region of the edge (Fig. 9a). We intersect the polygon with the region contained by the normals and the edge to obtain the stability region in  $O(n)$  time for a polygon with  $n$  edges. Any center of mass location in the interior of the stability region guarantees stability of the edge.

Uncertainty in the length, position, and orientation of an edge and in the position of the center of mass leads us to instead use the *shrunk stability region* and the *expanded stability region*. The shrunk stability region is a subset of the stability region, which is in turn a subset of the expanded stability region. We compute these regions using region intersection and union operations. (See Nievergelt and Preparata 1982 for region intersection and union algorithms.)

### 6.1. Shrunk Stability Region

The shrunk stability region of an edge is the set of nominal center of mass locations in the polygon interior for which the edge is always stable. The uncertainty in the length, location, and orientation of the edge, and uncertainty in the center of mass location, shrink the set of nominal center of mass locations for which the edge is guaranteed to be stable. The shrunk stability region is the intersection of the stability regions generated for every instance of the edge length, position, and orientation, further shrunk by the center of mass uncertainty radius.

Conceptually, the shrunk stability region of an edge can be obtained as follows. First, compute the stability region of every instantiation of the edge considering only the uncertainty in the vertex locations. Then, compute the intersection of the stability regions of all the instantiations of the edge and the polygon shrunk by  $r_v$ , the vertex uncertainty disk radius. Finally, shrink the resulting region by the center of mass uncertainty disk radius,  $r_c$ , to obtain the shrunk stability region.

Since the above procedure requires region intersection operations for every valid instantiation of the edge, we use a simpler procedure to compute a conservative approximation of the shrunk stability region. We identify the stability region valid for all edge instantiations and shrink it for the uncertainty in the center of mass location. Consider a nominal edge  $e$ . Let the nominal edge intersect the vertex uncertainty disks centered at its CW and CCW vertices at points  $P_{cw}$  and  $P_{ccw}$ , respectively. Translate the nominal edge segment inward by  $r_v$  and call it  $e'$ . Draw the two common separating tangents to the vertex uncertainty disks of the edge  $e$ ,  $t^{\min}$  and  $t^{\max}$ , which correspond to the minimum and maximum edge orientations, respectively (Fig. 9b). Consider the tangent  $t^{\min}$ . Erect the inward pointing normals  $n_{cw}^{\min}$  and  $n_{ccw}^{\min}$  to the tangent that pass through the points  $P_{cw}$  and  $P_{ccw}$ , respectively. Find the region  $R^{\min}$  formed by intersecting the inward halfplanes defined by the lines  $n_{cw}^{\min}$ ,  $n_{ccw}^{\min}$ , and  $e'$ .



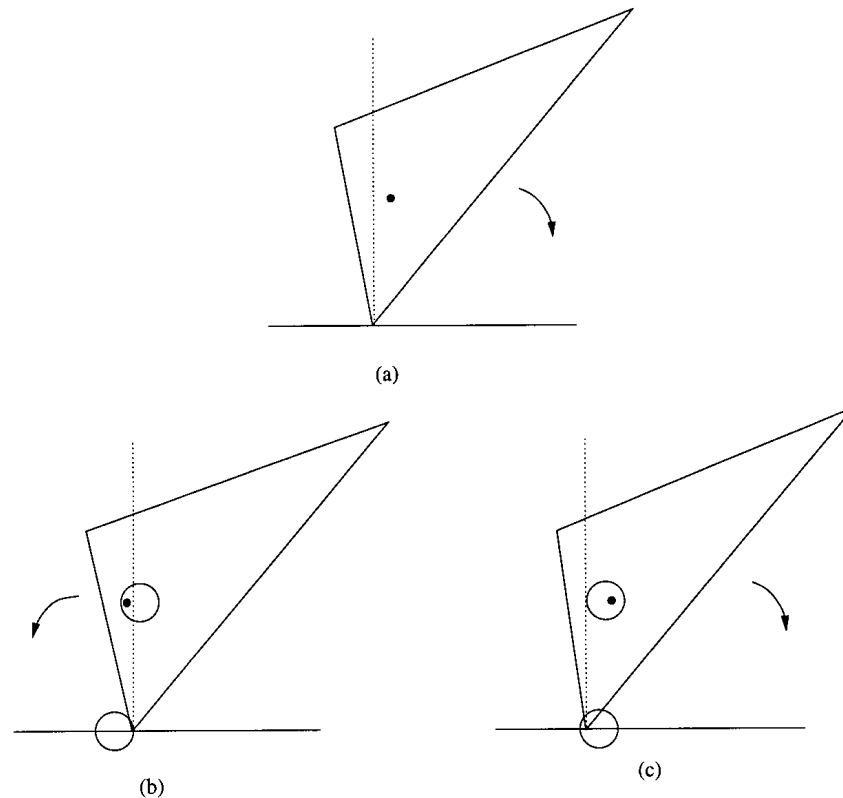


Fig. 7. Shape uncertainty results in nondeterministic actions. The result of the push depends on the relative location of the center of mass and contact vertex. The contact normal at the vertex is indicated by the dotted line. (a) For the nominal part shape, the line from the center of mass to the vertex is clockwise (CW) to the normal, and the part rotates CW. (b) The part rotates counterclockwise (CCW) for this instantiation of the part shape. (c) The part rotates CW for this instantiation of the part shape. The center of mass and vertex uncertainty disks are shown for the tolerated part instantiations.

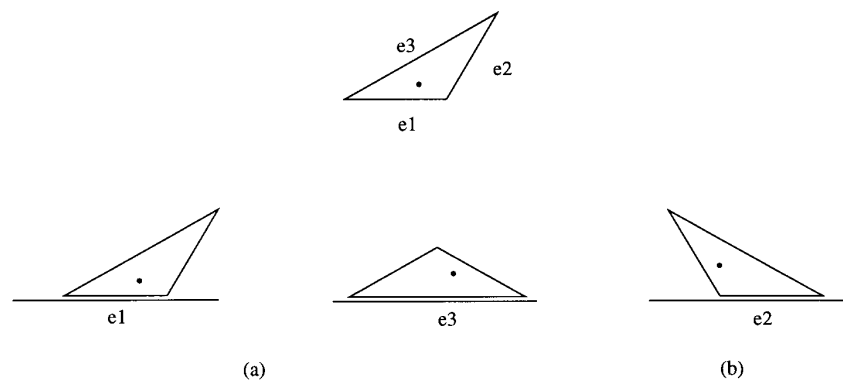


Fig. 8. Edges of a part can become stable or unstable depending on the part shape instantiation. (a) The isosceles triangle has stable edges  $e_1$  and  $e_3$  for its nominal shape. (b) Edge  $e_2$  can be stable for some instantiations of the tolerated part.

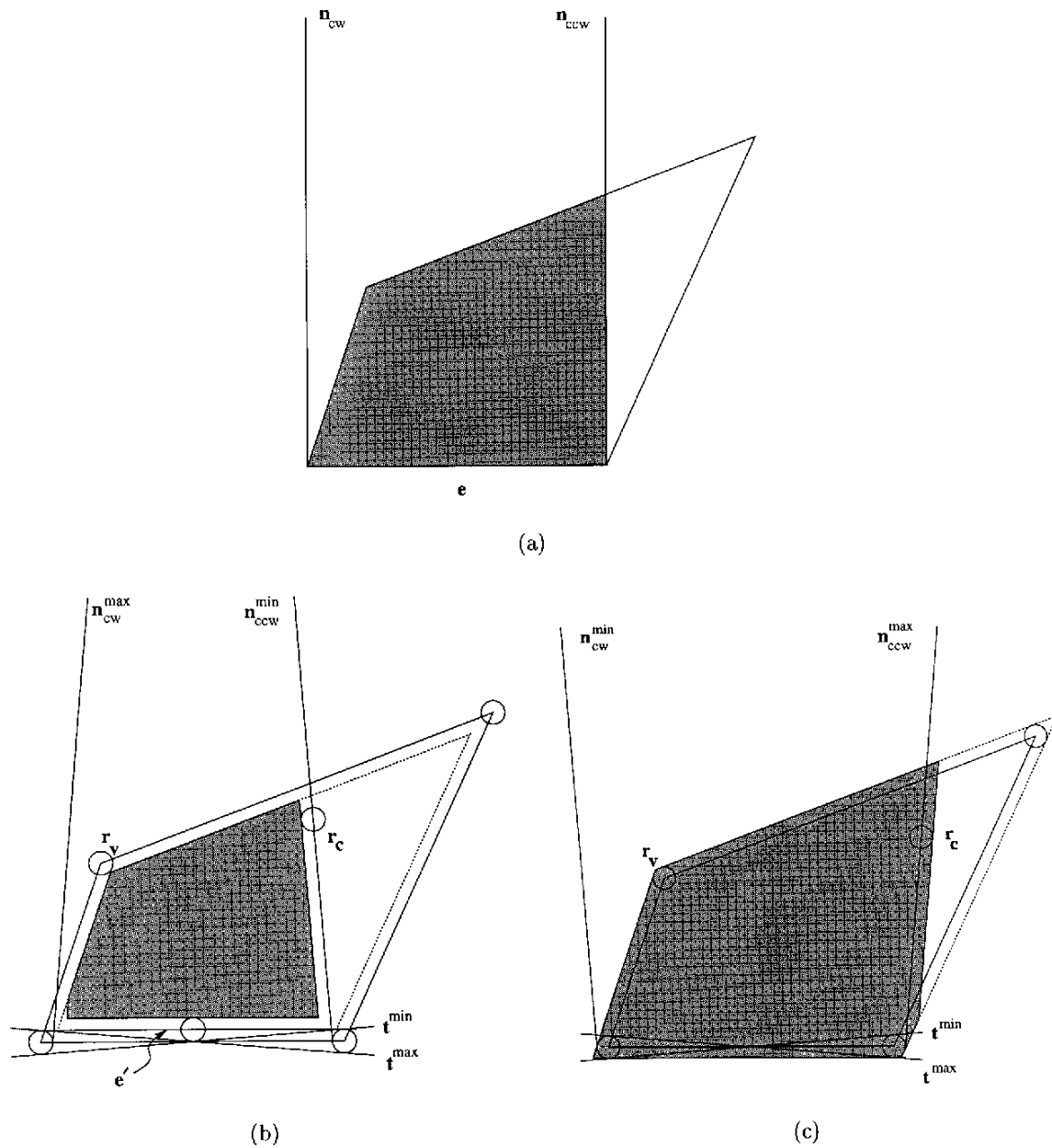


Fig. 9. Stability regions of the bottom-most edge  $e$  of the polygon. (a) Stability region with no shape uncertainty. (b) Shrunk stability region. (c) Expanded stability region. The shrunk and expanded stability regions shown here are conservative approximations of the true regions.

Repeat this operation for the other tangent  $t^{\max}$  to obtain the region  $R^{\max}$ . Shrink the polygon by  $r_v$  and intersect it with the intersection of  $R^{\min}$  and  $R^{\max}$ . Shrink this resultant region along the lines  $e'$ ,  $n_{cw}^{\max}$ , and  $n_{ccw}^{\min}$  by  $r_c$ , the center of mass uncertainty, to get a conservative approximation of the shrunken stability region of the edge.

Every instantiation of the edge is stable for any nominal center of mass location in the interior of the region computed above since the perpendicular projection of any valid center of mass lies in the interior of every possible edge instantiation. The CW and CCW boundaries of the shrunken stability region can be obtained from  $n_{cw}^{\max}$  and  $n_{ccw}^{\min}$ , respectively. Generate the lines  $e'$ ,  $n_{cw}^{\max}$ , and  $n_{ccw}^{\min}$ , shrink them inward by the amount  $r_c$ , and intersect the inward halfplanes defined by these lines with the polygon shrunk by  $r_v$  to obtain the (approximate) shrunken stability region. These operations can be performed in  $O(n)$  time for a polygon with  $n$  edges.

## 6.2. Expanded Stability Region

The expanded stability region of an edge is the set of all nominal center of mass locations in the interior of the polygon grown by  $r_v$  for which the edge may be stable. In contrast to the shrunken stability region, it is the union of the stability regions generated for every instance of the edge length, position, and orientation, further expanded by the center of mass uncertainty. The uncertainty in the positions of the vertices and the center of mass therefore enlarges the region of nominal center of mass locations for which the edge may be stable.

We compute a conservative approximation of the expanded stability region (Fig. 9c) that is guaranteed to include the exact expanded stability region. Draw the two common separating tangents to the vertex uncertainty disks of the nominal edge  $e$ ,  $t^{\min}$  and  $t^{\max}$ , which correspond to the extremal edge orientations. Consider the tangent  $t^{\min}$ . Erect the inward normals  $n_{cw}^{\min}$  and  $n_{ccw}^{\min}$  to the tangent that are also tangent to the vertex uncertainty disks of the edge and farthest from each other. (Note that these normals differ from those used to compute the shrunken stability region.) Move the edge line outward, away from the polygon interior, by  $r_v$ , and move the normals outward by the amount  $r_c$ . Find the region  $R^{\min}$  formed by the intersection of the inward halfplanes defined by these lines. Repeat this operation for the other tangent  $t^{\max}$  to obtain the region  $R^{\max}$ . Grow the polygon by  $r_v$  and intersect it with the union of  $R^{\min}$  and  $R^{\max}$ . The resulting region is the (approximate) expanded stability region of the edge.

The CW boundary of the expanded stability region can be obtained from  $n_{cw}^{\min}$ , and its CCW boundary can be obtained from  $n_{ccw}^{\max}$ . Move the edge line outward by  $r_v$ , and move the normals  $n_{cw}^{\min}$  and  $n_{ccw}^{\max}$  outward by the amount  $r_c$ . Intersect the inward halfplanes defined by these lines with the polygon expanded by  $r_v$  to obtain the (approximate) expanded stability region. This can be performed in  $O(n)$  time.

## 6.3. Edge Classification

If the nominal center of mass is inside the shrunken stability region of an edge, the edge is always stable. If the nominal center of mass is outside the expanded stability region of an edge, the edge is always unstable. When the nominal center of mass is outside the shrunken stability region and inside the expanded stability region, the edge may be stable or unstable depending on the instantiated part shape.

Given a nominal center of mass location, we can perform point-inclusion tests to determine if it is in the interior of the shrunken stability and expanded stability regions. (See Preparata and Shamos's 1985 book for a description of point-inclusion algorithms.) These tests identify an edge as always stable, always unstable, or sometimes stable. The point-inclusion test for the center of mass can be done in  $O(\log n)$  time since the stability region of an edge is convex. We can therefore identify the stability status of all the edges of the polygon in  $O(n \log n)$  time.

We first concentrate on parts whose set of stable edges is constant. We refer to a part with a constant set of stable edges for a given set of tolerance values as a part with a *single qualitative shape*. A part has a single qualitative shape when its nominal center of mass is inside the shrunken stability regions of all the stable edges and outside the expanded stability regions of all other edges for a given set of uncertainty values. For a part with a single qualitative shape, we can identify representative actions and generate plans using breadth-first search. These actions may be deterministic or nondeterministic, and we next describe how to generate them.

# 7. Generating Actions

Shape uncertainty introduces nondeterminism in the actions. To compute the deterministic and nondeterministic action ranges, for each start edge we find the smallest and largest rotations that are guaranteed to achieve the transition to each destination edge, and the smallest and largest rotations that can potentially achieve the transition to each destination edge. When computing these extremal actions for each edge, we assume that the following can occur simultaneously: the start edge can be in any orientation in its allowed range, each vertex can be anywhere in its uncertainty disk, and the center of mass can be anywhere in its uncertainty disk. From the extremal action ranges, we can find the representative actions for any given set of edges and search for an orienting plan using these actions. If a plan exists, it is guaranteed to work for any instance of the part since it works for any combination of center of mass, vertex, and edge placements.

## 7.1. Deterministic Action Ranges

Consider transitioning from state  $s_i$  to state  $s_j$  with shape uncertainty. There are variations in the stable orientation and in the resting range of each edge (Figs. 10 and 11). We

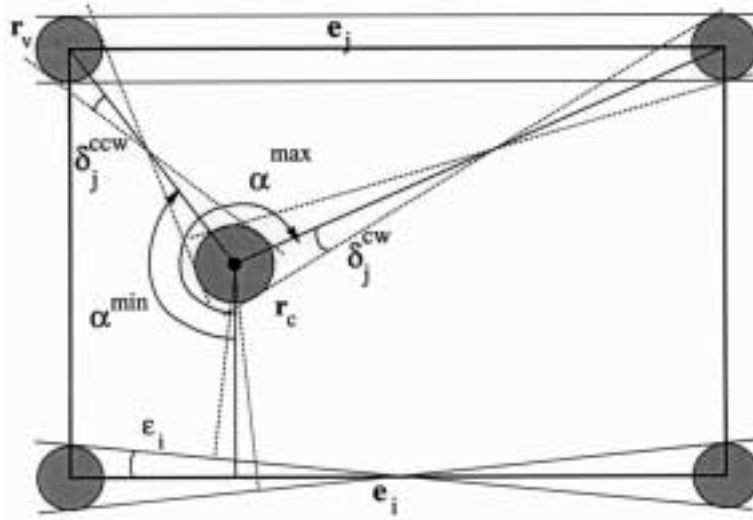


Fig. 10. The uncertainty in stable orientations and resting ranges of the edges due to shape uncertainty modifies the action ranges for the transition from edge  $e_i$  to edge  $e_j$ .

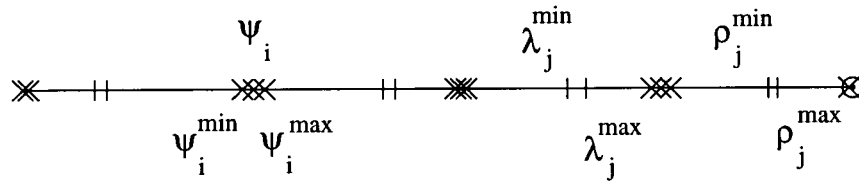


Fig. 11. The uncertainty in stable orientations and resting ranges of edges due to shape uncertainty is indicated for the states  $s_i$  and  $s_j$ .

determine these variations from the uncertainty disks of the center of mass and the *transition vertices*. A transition vertex is a polygon vertex that corresponds to a local maximum in the radius function and so specifies the limit of a resting range. The stable orientation  $\psi_i$  of state  $s_i$  varies between  $\psi_i^{min}$  and  $\psi_i^{max}$ , where  $\psi_i^{min} = \psi_i - \epsilon_i$ ,  $\psi_i^{max} = \psi_i + \epsilon_i$ ,  $\epsilon_i = \sin^{-1}(2r_v/l_i)$ , and  $l_i$  is the nominal length of edge  $e_i$ . The right limit of the resting range of state  $s_j$  varies between  $\rho_j^{min}$  and  $\rho_j^{max}$ , and this variation is computed from  $r_v$ ,  $r_c$ , and the distance  $d_j^{cw}$  from the center of mass to the CW transition vertex for the edge. The minimum limit  $\rho_j^{min}$  is given by  $\rho_j - \delta_j^{cw}$ , and the maximum limit  $\rho_j^{max}$  is given by  $\rho_j + \delta_j^{cw}$ , where  $\delta_j^{cw} = \sin^{-1}((r_v + r_c)/d_j^{cw})$ . Similarly, the left limit of the resting range of state  $s_j$  varies from  $\lambda_j^{min} = \lambda_j - \delta_j^{ccw}$  to  $\lambda_j^{max} = \lambda_j + \delta_j^{ccw}$ , where  $\delta_j^{ccw} = \sin^{-1}((r_v + r_c)/d_j^{ccw})$  and  $d_j^{ccw}$  is the distance from the center of mass to the CCW transition vertex for the edge. See the example in Figure 12.

The action range specified by the open interval  $(\lambda_j^{max} - \psi_i^{min}, \rho_j^{min} - \psi_i^{max})$  guarantees a deterministic transition from  $s_i$  to  $s_j$ . A deterministic action range is an equivalence

class of actions. So uncertainty in part shape causes the deterministic action range to shrink from  $(\lambda_j - \psi_i, \rho_j - \psi_i)$  to  $(\lambda_j^{max} - \psi_i^{min}, \rho_j^{min} - \psi_i^{max})$  as shown in Figure 13, or equivalently, to shrink from  $(\alpha^{min}, \alpha^{max})$  to  $(\alpha^{min} + \epsilon_i + \delta_j^{ccw}, \alpha^{max} - \epsilon_i - \delta_j^{cw})$ . In fact, deterministic action ranges can vanish for large enough values of uncertainty, when  $\lambda_j^{max} - \psi_i^{min} \geq \rho_j^{min} - \psi_i^{max}$ . Intuitively, this occurs when the uncertainty in the stable orientation of the start edge is as large or larger than the minimal resting range of the edge it is transitioning to. When this occurs, the deterministic action ranges are no longer guaranteed to cover the action space of  $[0, 360)$  and there may not be deterministic actions to get from every state to every other state. In such cases, a plan to orient the part using only deterministic actions may not exist.

## 7.2. Nondeterministic Action Ranges

Nondeterministic action ranges are action ranges with multiple possible outcomes due to shape uncertainty. A nondeterministic action causes a transition from a start edge to a destination edge or the stable edges adjacent to the destination

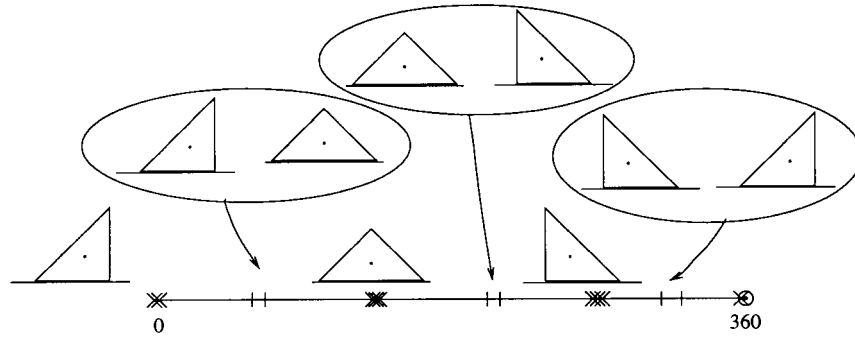


Fig. 12. Resting ranges for an isosceles right triangle with shape uncertainty.  $r_v$  and  $r_c$  are 0.4 mm and the hypotenuse of the triangle has a length of 22.63 mm. The uncertainty in the stable orientations is indicated by the x's drawn at the nominal and extremal orientations, and uncertainty in the resting ranges is indicated by the vertical bars drawn at the extremal range limits.

edge. We compute the nondeterministic action ranges from state  $s_i$  that can lead to state  $s_j$  or its CW or CCW stable neighbors,  $s_j^{cw}$  and  $s_j^{ccw}$ , respectively (Fig. 13). The action range specified by the closed interval  $[\lambda_j^{\min} - \psi_i^{\max}, \lambda_j^{\max} - \psi_i^{\min}]$  is the range of actions for which the part transitions from state  $s_i$  to either state  $s_j$  or state  $s_j^{ccw}$  and  $[\rho_j^{\min} - \psi_i^{\max}, \rho_j^{\max} - \psi_i^{\min}]$  is the range of actions for which the part transitions from state  $s_i$  to either state  $s_j$  or state  $s_j^{cw}$ . So the nondeterministic action ranges  $[\alpha^{\min} - \epsilon_i - \delta_j^{ccw}, \alpha^{\min} + \epsilon_i + \delta_j^{cw}]$  and  $[\alpha^{\max} - \epsilon_i - \delta_j^{cw}, \alpha^{\max} + \epsilon_i + \delta_j^{ccw}]$  bracket the deterministic action range  $(\alpha^{\min} + \epsilon_i + \delta_j^{ccw}, \alpha^{\max} - \epsilon_i - \delta_j^{cw})$ . A nondeterministic action range is not guaranteed to be an equivalence class of actions.

### 7.3. Overlap Ranges for a Set of States

The deterministic and nondeterministic action ranges for transitions from a state to the other states cover the entire action space of  $[0, 360)$ , as illustrated in Figure 14. To find the deterministic and nondeterministic action ranges of a set of states, we first compute the deterministic and nondeterministic action ranges of each individual state in the set. We overlap the set of action range intervals from the individual states to obtain another set of intervals, the *overlap ranges*. Overlap ranges formed by the overlap of only deterministic action ranges are deterministic overlap ranges, and overlap ranges formed by the overlap of at least one nondeterministic action range are nondeterministic overlap ranges. Representative deterministic and nondeterministic actions are selected from the middle of deterministic and nondeterministic overlap ranges, respectively.

## 8. Sensor-Based Orienting with Shape Uncertainty

Planning in the presence of shape uncertainty is a difficult problem since we must find plans that work for the infinite

set of part shapes that are all valid instances of the variational class (Fig. 15). Since the deterministic action ranges do not cover the space of actions, using only deterministic actions may not yield a plan even when one exists (Fig. 16). We use both deterministic and nondeterministic actions to guarantee the action space is covered and generate plans by breadth-first search of an AND/OR graph.

### 8.1. AND/OR Search

We find an orienting plan by performing breadth-first AND/OR search. (See Rich and Knight 1991 for a description of AND/OR graphs and the similar AO\* algorithm.) The root node contains the set of all possible initial orientations of the part. A node in the search graph contains the set of orientations consistent with the push-align operations along the path from the root to the node. Each alternative (OR) push-align operation corresponds to a link. When a push-align operation is applied at a node, all stable orientations that can result are classified into sets of indistinguishable states, based on their diameters. The AND link from a node for a given operation points to a set of child nodes where each child node contains a set of indistinguishable states.

To deal with variations in the diameter values due to shape uncertainty, for each stable state compute the range of diameter values it can assume and the corresponding range of sensor values. Two states are considered *distinguishable* if their ranges of sensor values do not overlap, and two states with overlapping ranges of sensor values are considered *indistinguishable*. We group the resulting states into indistinguishable sets by sorting them by their nominal diameter values and testing neighboring states for distinguishability.

When computing the action ranges for a state, we also store the resulting set of states for each action range. When an action is applied to a given set of initial states, we find the action range that the action belongs to for each of the initial states and retrieve the corresponding stored resulting states. The union of the resulting states for all the initial states is the resulting set of states for the specified action and initial states.



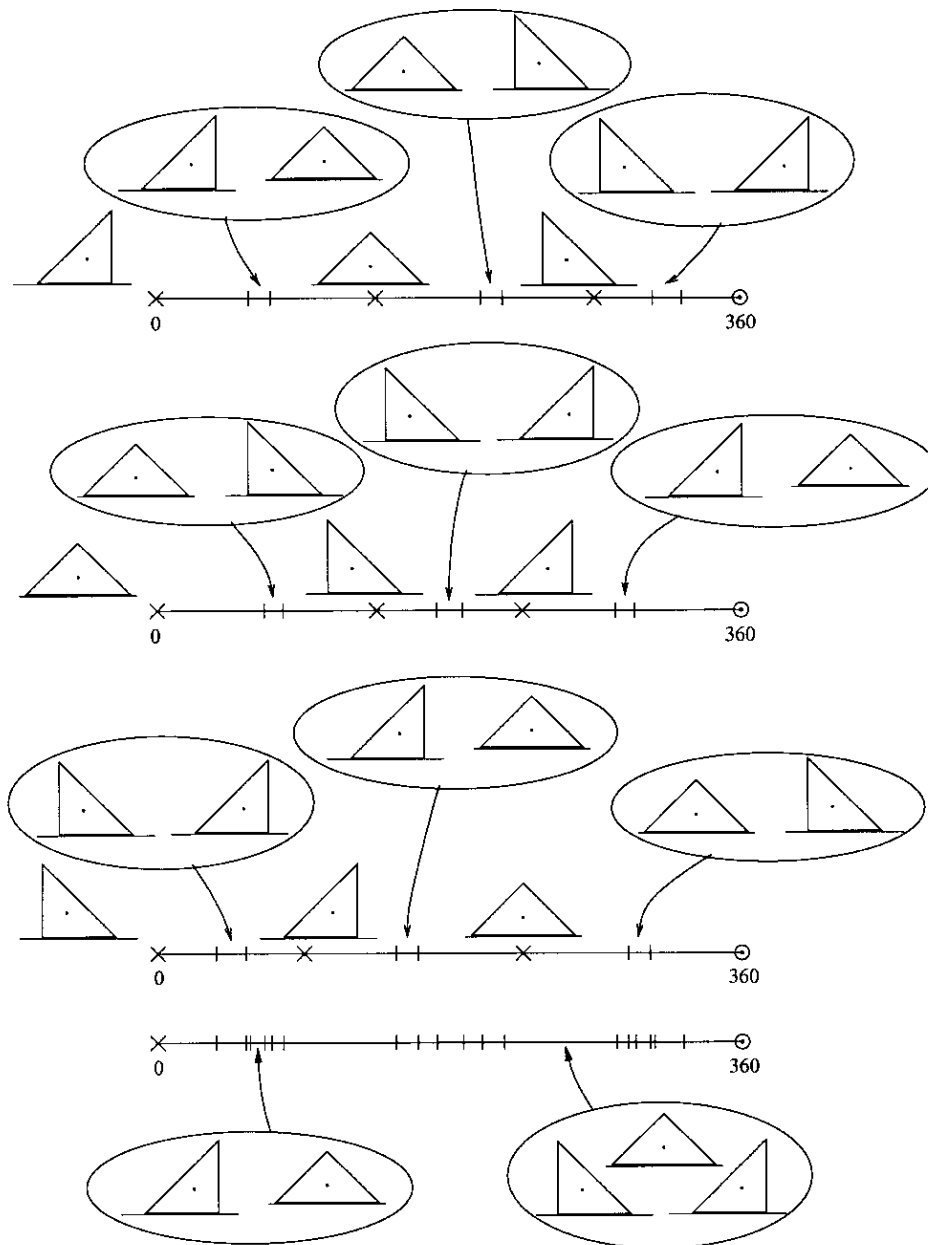


Fig. 13. Action ranges with shape uncertainty for the states shown at left, for the triangle of Figure 12. Only the nominal stable orientations, represented by an x, are shown for clarity. Each action range that contains an x and is bracketed by a pair of successive vertical bars is a deterministic action range, and each action range that does not contain an x and is bracketed by a pair of successive vertical bars is a nondeterministic action range. The resulting state for each deterministic action range and the set of possible states for each nondeterministic action range are also shown. The overlap ranges for the three stable edges of the triangle are indicated at the bottom.

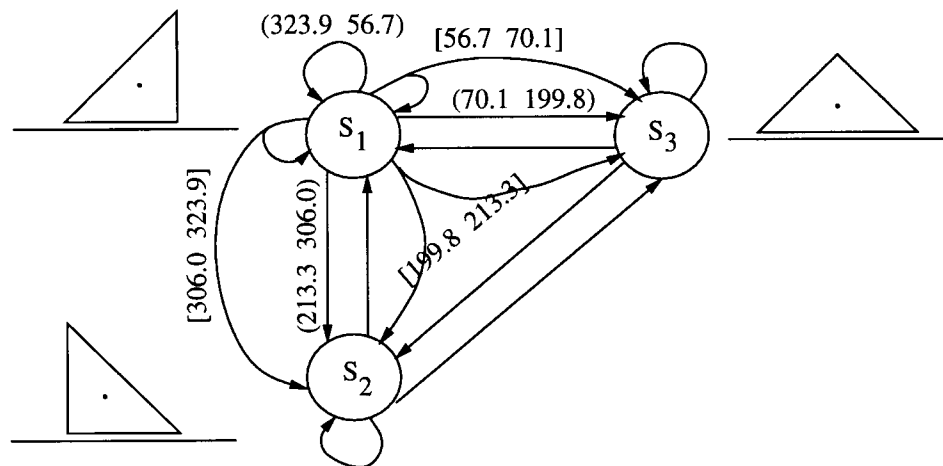


Fig. 14. State transition graph of the isosceles right triangle with nondeterministic and deterministic action ranges. For clarity, nondeterministic arcs and action ranges are shown only for transitions from state  $s_1$ .  $r_c$  and  $r_v$  are 0.4 mm, and the hypotenuse has length 22.63 mm.

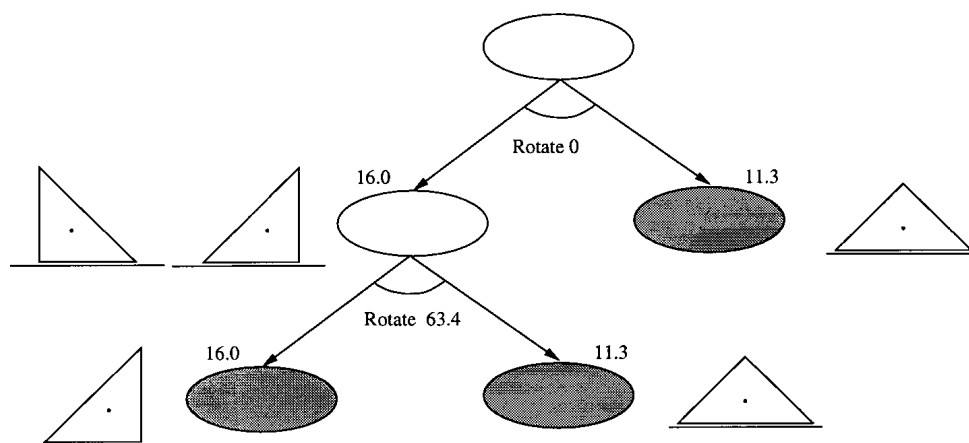


Fig. 15. A sensor-based plan to orient the isosceles right triangle, when  $r_v$  and  $r_c$  are 0.4 mm. The arrows linked by an arc represent a push-align operation. Each node contains a set of indistinguishable states, and the sensor value shown at the node indicates their average diameter value. Goal nodes, shown shaded, have a single orientation.

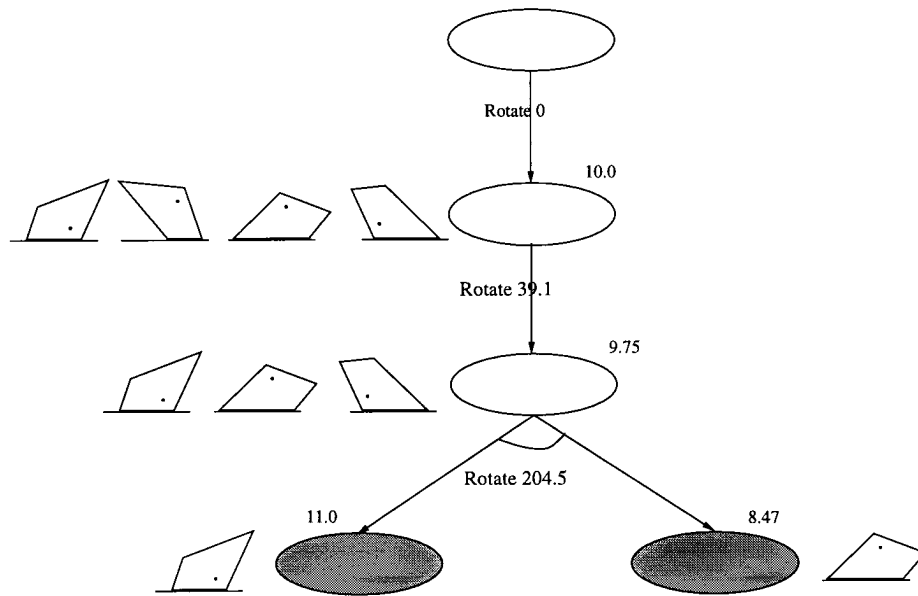


Fig. 16. A plan using nondeterministic and deterministic actions exists for the quadrilateral when no plan using only deterministic actions exists.  $r_v$  and  $r_c$  are 0.5 mm, and the longest polygon edge has length 13.93 mm.

Search begins at the root node. The first push-align operation results in a set of nodes that are the indistinguishable sets of stable states. The search explores the nodes in a breadth-first manner by applying the representative actions for their constituent states to generate their child nodes. A node is solved if it is a goal node with a single state or when all its child nodes from an operation are solved. When a node is solved, its parent nodes are updated. Search terminates when the root node is solved or all nodes have been explored. The generated plan consists of a conditional sequence of operations to determine part orientation. The search process is exhaustive, but it need be performed offline only once for each part and it returns the minimum length plan for the computed action ranges. See Figure 17 for an example plan.

## 8.2. Plan Characteristics

We first ask if there always exists a guaranteed plan to orient any part that satisfies the tolerance model. We show that plan existence for a known part shape does not imply existence of a guaranteed plan for a toleranced part. Consider a rectangle with its center of mass at a distance  $d$  from its geometric center and whose nominal breadth  $b$ , nominal height  $h$ , vertex uncertainty disk radius  $r_v$ , and center of mass uncertainty disk radius  $r_c$  are chosen such that  $b > h$ ,  $b - 2r_v \leq h + 2r_v$ , and  $d < r_c$ . The nominal rectangle can be brought to a distinct orientation. A valid instantiation of this rectangle with shape uncertainty is a square with its center of mass at its geometric center, and such a square can be oriented only up to symmetry.

Any part with at least one stable edge with a unique diameter value can be oriented, at least by a randomized plan

that repeatedly performs random rotations of the part until it comes to rest on the stable edge with the unique value.

Although the generated plans are the minimum length plans for the computed action ranges, the plan length for a toleranced part can exceed the plan length bounds for orienting a known part shape obtained in Akella and Mason (1999). See the example in Figure 18.

## 9. Sensorless Orienting with Shape Uncertainty

We now show that sensorless orienting of a part with shape uncertainty is possible. A sensorless plan must bring all initial part orientations to the same goal orientation. A planner can generate sensorless plans using breadth-first search with deterministic and nondeterministic actions. See Figure 19 for an example sensorless plan. The planner generates minimum length sensorless orienting plans for the computed action ranges. If a sensorless plan exists for a given set of uncertainty values, a sensor-based plan also exists for those values. However, the converse is not true. Furthermore, the length of the sensorless plan provides an upper bound on the length of the sensor-based plan.

In recent work, Chen et al. (1998) generate sensorless orienting plans for a class of toleranced polygonal parts by modifying the algorithm of Chen and Ierardi (1995) for sensorless orienting of a known part. They show that a sensorless plan exists for any part that has a stable edge  $e_i$  with a uniquely maximal transition angle  $\alpha_i^{\text{trans}}$  to a neighboring stable edge. A finite number of repeated applications of an action  $\alpha^{\text{repeat}}$ , chosen so that  $\alpha_i^{\text{trans}} > \alpha^{\text{repeat}} > \max(\alpha_j^{\text{trans}})$ ,  $j \neq i$ , causes all initial states  $s_j$  to transition to and be trapped in state  $s_i$ . If

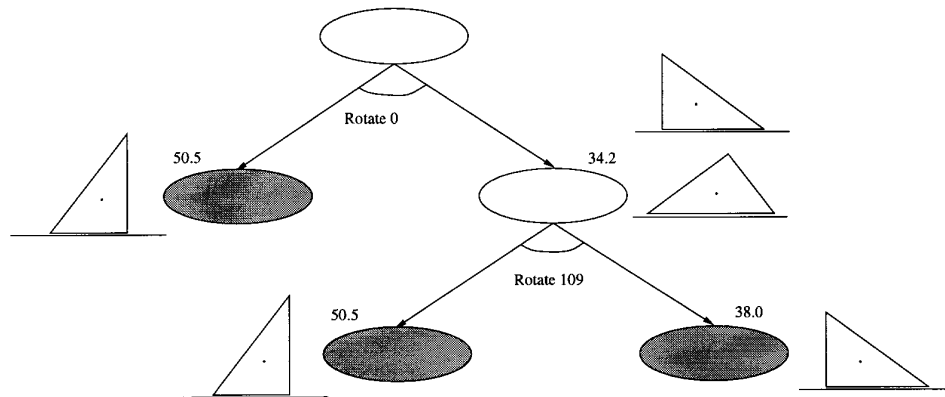


Fig. 17. Sensor-based plan with shape uncertainty for a right triangle.  $r_c$  and  $r_v$  are 2 mm, and the longest edge has length 63.2 mm.

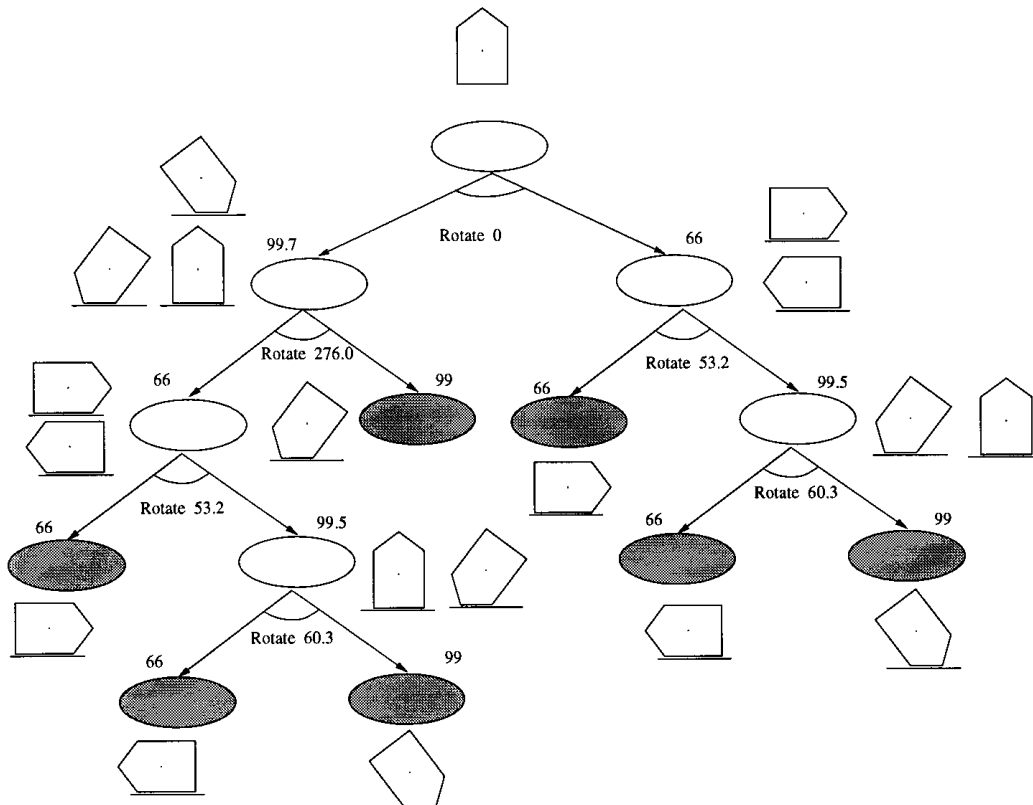


Fig. 18. A sensor-based orienting plan for a toleranced part that does not satisfy the plan length bounds for its nominal shape. This is a four-step plan, and the plan length for its nominal shape is three steps.  $r_v$  is 0.75 mm,  $r_c$  is 1 mm, and the longest edge has length 75 mm.

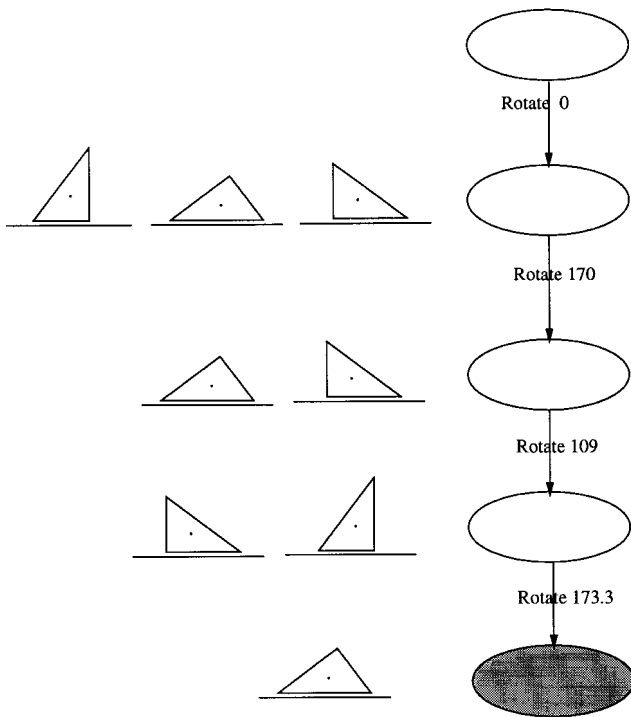


Fig. 19. Sensorless plan with shape uncertainty for the right triangle of Figure 17.  $r_c$  and  $r_v$  are 2 mm, and the longest edge has length 63.2 mm. Each node contains a set of stable states, and each arrow represents an action. The shaded goal node contains a single state. This plan is one step longer than the sensorless plan with no shape uncertainty.

computation of  $\alpha_i^{\text{trans}}$  accounts for center of mass uncertainty, this algorithm can find sensorless plans for parts under our tolerance model that satisfy the above maximality condition, even if their set of stable edges changes. However, these may not be minimum length plans since they use a single action repeatedly.

## 10. Are the Planners Complete?

Since the existence of a plan for a nominal shape does not guarantee existence of a plan for the toleranced shape, we address the question of planner completeness here: given a nominal part shape with bounded shape uncertainty that satisfies our assumptions, does the planner always return an orienting plan when one exists and indicate failure when no such plan exists?

We first consider completeness of the sensor-based planner. Using our tolerance model, the planner computes deterministic and nondeterministic action ranges, which cover the interval  $[0, 360)$ . The planner chooses representative actions from the overlap ranges obtained from these action ranges and generates plans by performing breadth-first search. The plan-

ner is complete if the computed action ranges are accurate. If the action ranges are computed conservatively, the planner may not find a solution even when one exists.

The deterministic and nondeterministic action ranges for a stable edge depend on its orientation range and the allowed positions of the center of mass and transition vertices. When generating the action ranges, we assume that the orientation of each stable edge can take any value in its allowed orientation range and that the center of mass and the transition vertices can be located anywhere in their uncertainty disks. We call this the *independence assumption* since we assume independence of the edge orientations and vertex positions. When a plan exists, it is guaranteed to work for any instance of the part since the generated actions permit any combination of center of mass and vertex positions.

Each instantiation of the part within the tolerance bounds is a shape with constraints on the orientations and positions of the part edges. For example, the sum of the interior angles of an  $n$ -gon must sum to  $(2n - 4)90$  degrees. Also, multiple edges cannot all be at their extremal orientations. These constraints suggest the action ranges generated under the independence assumption are overly conservative.

Consider a stable edge, the start edge, whose action ranges are to be computed. For a given orientation of the start edge, the positions of only its vertices are constrained. Any other vertex can assume any position in its uncertainty disk for any given orientation of the start edge. So the action ranges from a stable edge to any other stable edge are accurately determined if the destination edge is neither an adjacent edge nor a nonadjacent edge with a transition vertex that belongs to the start edge. For transitions from the start edge to either an adjacent edge or a nonadjacent edge whose transition vertex it contains, we can find the extremal position ranges of the vertices for each orientation of the start edge and compute the corresponding action ranges. For example, when the edge is in an extremal orientation, there is exactly one set of positions its vertices can assume. The union of the action ranges over all orientations of the edge gives the maximal action range for the transition. The computed action ranges to adjacent edges and nonadjacent edges with a shared transition vertex under the independence assumption are more conservative than those computed by this procedure.

The accuracy with which we determine the locus of the center of mass also determines the accuracy of the action ranges. We have assumed that the center of mass uncertainty locus is described by a disk. In fact, this locus is not constrained to be a circle for a polygon with uniform density, as illustrated in the appendix. The circumscribing circle we use may be an overly conservative approximation of the true locus.

These two sources of inaccuracy in the action ranges mean that our planner may not be complete. When the planner generates a plan, all instances of the part are guaranteed to be orientable. When the planner cannot find a plan, however, it is unclear if there exist part instantiations that cannot be



oriented. Completeness of the sensorless planner, as with the sensor-based planner, depends on the accuracy of the action ranges.

## 11. Multiple Qualitative Shapes

We have so far assumed that the set of stable edges stays constant over all instantiations of the tolerance parameters. When the set of stable edges can change due to shape uncertainty, a part can exhibit qualitatively different mechanical behaviors. For example, a part with two stable edges in its nominal shape can behave like a part with three stable edges for some instantiations of its variational class. This occurs when the nominal center of mass is in the expanded stability region of at least one edge without also being in its shrunken stability region. We refer to a part whose set of stable edges can vary as a part with *multiple qualitative shapes* and refer to an edge that can be stable or unstable depending on the particular shape instantiation as a *sometimes-stable edge*. A plan generated for one qualitative shape of a part with multiple qualitative shapes may fail for another qualitative shape of the part (Fig. 20).

Interestingly, plans that work even in the presence of qualitative shape changes can sometimes be found. See Figure 21 for such an example plan. Qualitative shape changes modify the orienting problem to one with multiple state transition graphs for each part, where each graph represents a different qualitative shape of the part (Fig. 22). Each state transition graph is a directed graph whose nodes are the appropriate stable and sometimes-stable edges. Each directed arc contains the action range for the transition from the state at its tail to the state(s) at its head. We must determine the action ranges associated with each of the arcs of the graphs and perform planning in the space of these multiple graphs. A guaranteed orienting plan is one that can successfully orient every part shape corresponding to any of the graphs.

A part can have multiple qualitative shapes for a given set of uncertainty values in the following cases:

1. The nominal center of mass is inside the shrunken stability regions of stable edges, inside the expanded stability regions of some other edges without being inside their shrunken stability regions, and outside the expanded stability regions of all remaining edges. See Figure 23(a) for an example.
2. The nominal center of mass is outside the shrunken stability regions of all edges, inside the expanded stability regions of some edges, and outside the expanded stability regions of the remaining edges. See Figure 23(b) for an example.

### 11.1. Generating Plans for Multiple Qualitative Shapes

We identify all qualitative shapes of a part by first identifying the set of stable, unstable, and sometimes-stable edges

by performing the point-inclusion test for the nominal center of mass with the shrunken and expanded stability regions of every edge as described in Section 6. Each qualitative shape is defined by all its stable edges and a distinct subset of the sometimes-stable edges. Since the stability of the sometimes-stable edges depends on the instantiated part shapes, we must find plans that work for any valid combination of stable edges. A part with  $s$  sometimes-stable edges has potentially  $2^s$  combinations of stable edges, and therefore up to  $2^s$  qualitative shapes and transition graphs.

We sketch the procedure to generate plans when there are multiple qualitative shapes for a part. For each qualitative shape, determine its resting ranges. Using the resting ranges, compute the action ranges for each stable and sometimes-stable state in each qualitative shape. For every state that is stable or sometimes stable, find its action ranges for each qualitative shape and compute its composite action ranges over all qualitative shapes by finding the overlapping action intervals just as we compute overlap ranges for parts with a single qualitative shape. Note that actions that belong to the composite action ranges can result in multiple outcomes—they are potentially nondeterministic. For a set of indistinguishable states, compute the corresponding overlap ranges using the composite action ranges for the individual states. From the overlap ranges, find representative actions and then perform breadth-first AND/OR search to find a plan.

## 12. Implementation

We implemented sensor-based and sensorless planners in Common Lisp for orienting toleranced polygonal parts that have a single qualitative shape. Given a nominal part shape, radius values of the center of mass and vertex uncertainty disks, and bounds on sensor noise, they return a plan when they can find one and indicate failure otherwise. Some example parts we tested the planners on are shown in Figure 24.

The sensor-based planner performs breadth-first AND/OR search to generate sensor-based orienting plans for toleranced parts. The planner uses both deterministic and nondeterministic actions. For the parts in Figure 24, going from top to bottom, left to right, the sensor-based planner took an average of 0.192 secs, 1.870 secs, 0.756 secs, 0.262 secs, 0.262 secs, 0.224 secs, and 0.188 secs, respectively, on a SPARC ELC.

The sensorless planner uses breadth-first search to find sensorless orienting plans with deterministic and nondeterministic actions. See Figure 19 for an example plan generated by the planner. Not surprisingly, sensor-based orienting plans typically work for larger values of the tolerance parameters than sensorless orienting plans.

We implemented and tested sensor-based and sensorless orienting plans with shape uncertainty using an Adept 550 robot and conveyor belt. The robot picks up singulated parts

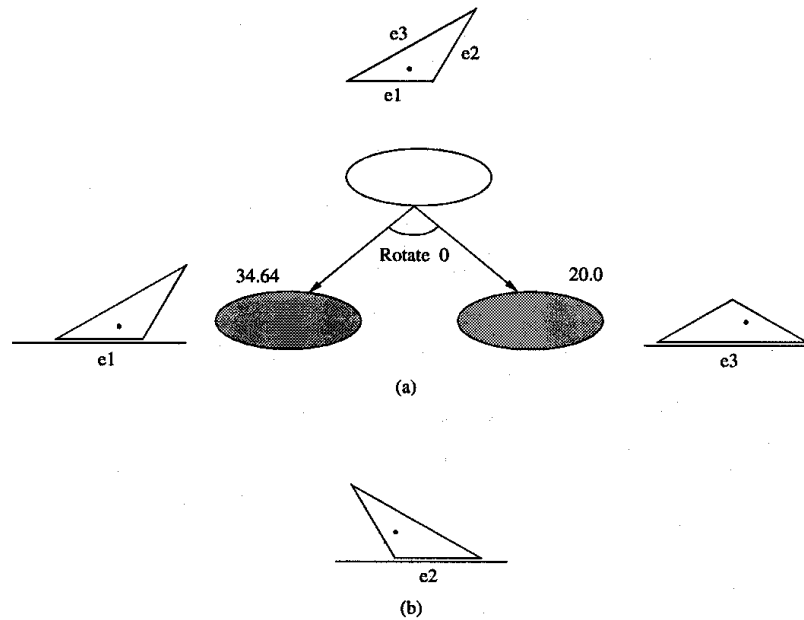


Fig. 20. The effect of qualitative shape changes due to shape uncertainty. (a) An orienting plan for the nominal part shape, for which edges  $e_1$  and  $e_3$  are stable and edge  $e_2$  is unstable. The longest edge  $e_3$  has length 69.28 mm. (b) For tolerance values  $r_v$  and  $r_c$  of 2 mm,  $e_1$  and  $e_3$  are always stable and  $e_2$  is stable for some instantiations. The plan fails for such instances since it cannot distinguish edges  $e_1$  and  $e_2$ , which have the same diameter value.

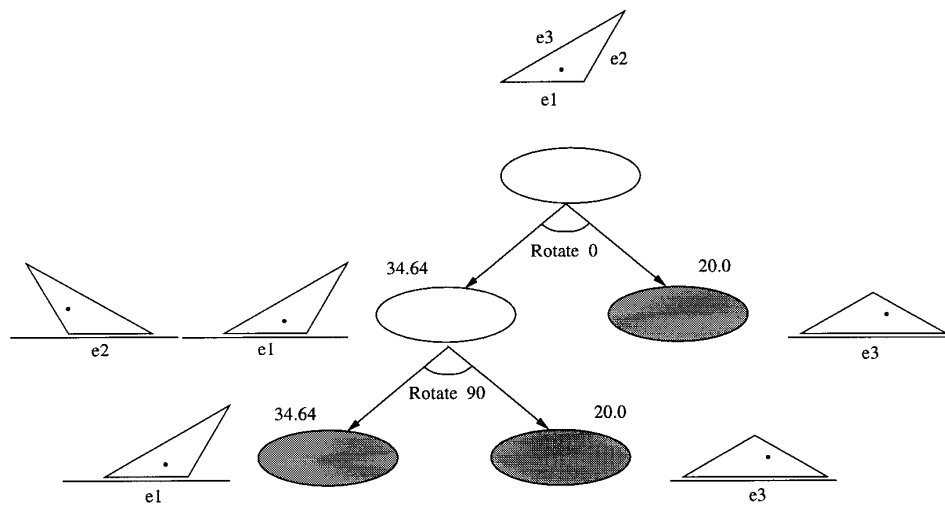


Fig. 21. A plan that works for the triangle of Figure 20 even with qualitative shape changes.

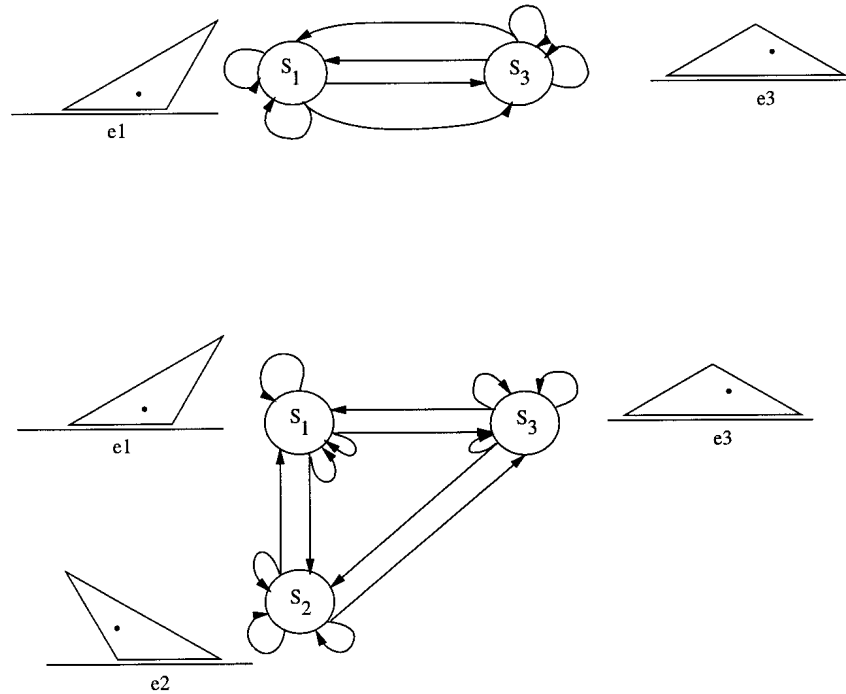


Fig. 22. Transition graphs for the two qualitative shapes of the triangle. Some of the directed arcs have been omitted for clarity. Edges  $e_1$  and  $e_3$  are always stable, and edge  $e_2$  is sometimes stable. The number of transition graphs grows exponentially with the number of sometimes-stable edges.

using a suction cup. A test set of triangles we used is shown in Figure 25. The parts and the fence were made of delrin. We ran 30 trials of the sensor-based plan (Fig. 17), with 10 trials for each part. We also ran 15 trials of the sensorless plan (Fig. 19), with 5 trials for each part. Both plans succeeded on all trials. During the experiments, we observed that nondeterministic actions typically take longer to execute since the center of mass lies closer to the contact normal. We therefore empirically selected appropriate push durations.

### 13. Conclusion

Developing techniques to manipulate parts manufactured to tolerances is important for automated manufacturing. In this paper, we characterized the effects of shape uncertainty on parts orienting and demonstrated that it is possible to orient tolerated polygonal parts. This work is among the first to explore the manipulation of parts with shape uncertainty. We have shown that the operational effect of shape uncertainty is to introduce nondeterminism. We characterized a class of tolerated parts that can be oriented, and we generated reliable sensor-based and sensorless orienting plans for these parts. Similar analyses can be applied to other orienting tasks whose action ranges can be computed, such as orienting with the sensorless IJOC (Akella et al. 1997), parallel-jaw grasping (Goldberg 1993), and tray tilting (Erdmann and Mason 1988).

Future work includes identifying alternative tolerance models that permit analysis of the effects of shape uncertainty on parts orienting while capturing shape variations in manufactured parts. To more faithfully model shape variations in manufactured parts, we might model a polygon edge as a sequence of connected line segments and specify vertex uncertainty disks with differing radii. In addition to experimental evaluation with industrial parts, broadening the applicable class of parts to include nonconvex parts, parts with curved edges, and 3-D parts is an important future objective.

Probabilistic modeling of the actions by empirical observation over a sample set of parts can reduce the need for analytical computation of the actions. See Christiansen (1992) and Brost and Christiansen (1996) for examples of tasks whose action probabilities are empirically estimated. Randomization during action selection, as advocated by Erdmann (1992) for manipulation tasks, is another approach. Randomization can be especially effective when several states have unique sensor values. We can also estimate the probability distributions of the initial part orientation and the tolerance parameters from knowledge of the manufacturing process, and generate plans that minimize the expected execution length. The worst-case length of a plan that minimizes expected length may, however, exceed that of the plan with the minimum worst-case length. Although it is tempting to model the orienting task as a partially observable Markov decision process with the part diameter as the partially observable variable, the

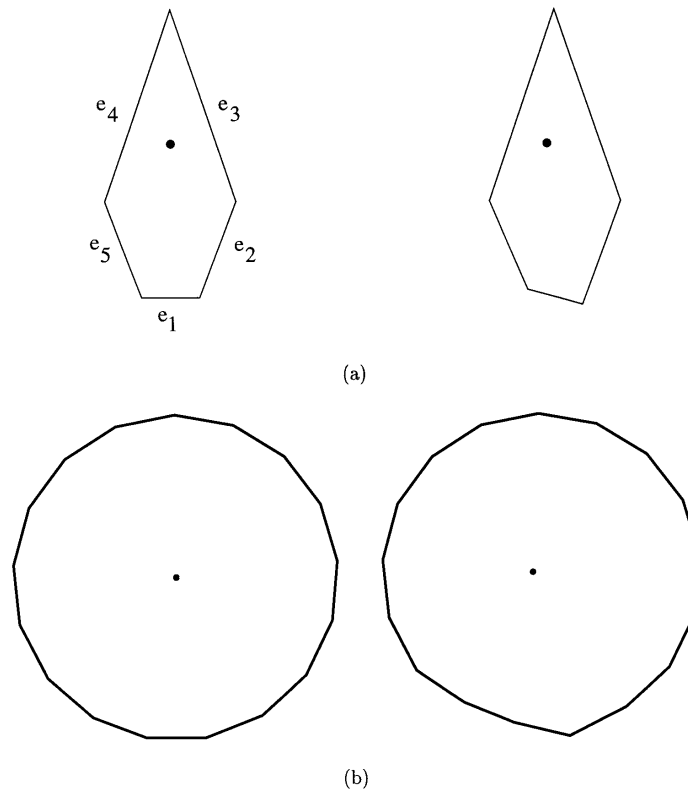


Fig. 23. Example parts that can undergo qualitative shape changes, with the nominal part on the left and a qualitatively different instantiation on the right. (a) A 5-gon with a single sometimes-stable edge. Edge  $e_1$  is sometimes stable,  $e_2$  and  $e_5$  are always unstable, and  $e_3$  and  $e_4$  are always stable for the specified tolerances. (b) A 17-gon whose edges are all sometimes stable. It was created by replicating the triangular wedge formed by edge  $e_1$  and the center of mass of the 5-gon 16 times, and adding a thinner wedge.

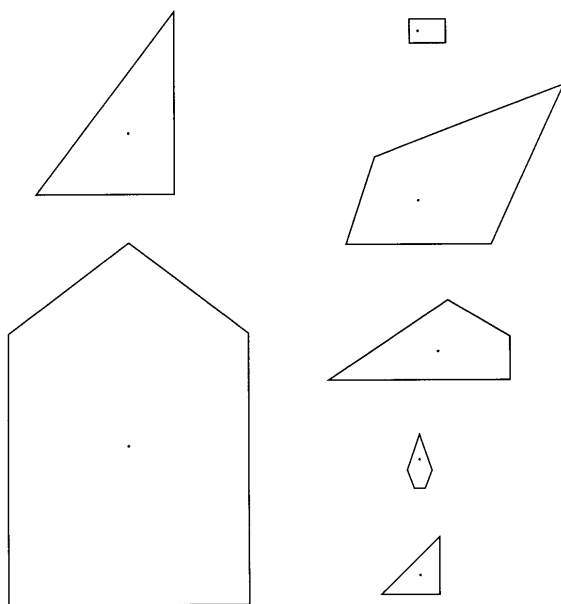


Fig. 24. Example part shapes with shape uncertainty that the planners were tested on.

orienting process is not Markovian. The transition probabilities of an edge are not independent of the transition probabilities of other edges, since they are related by part geometry.

Computing the maximum tolerances for which a plan exists is important. We can obtain conservative bounds on the maximum tolerances by finding the largest center of mass uncertainty radius that yields a plan with the vertex uncertainty set to zero, and vice versa. Determining the center of mass locus accurately is important in this context. To extend the class of plans beyond guaranteed plans, it would be useful to develop planners that generate plans that either orient a part or recognize when they cannot orient the part. Such plans, similar to Donald's (1989) error detection and recovery (EDR) plans for motion planning under uncertainty, are especially useful when we cannot find a guaranteed plan for a part. Such plans can potentially handle larger values of shape uncertainty and a broader class of parts. They may even be used as metrological tools to identify and eliminate parts that do not meet tolerance specifications.

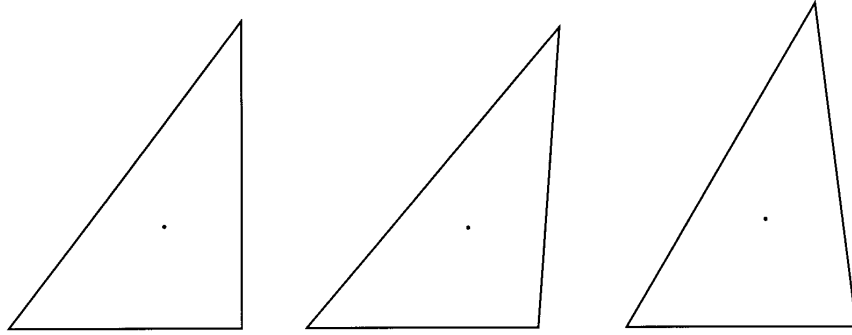


Fig. 25. Part shapes used in experiments to test plans with shape uncertainty. Going left to right, the nominal triangle, triangle with  $r_v$  and  $r_c$  of 1 mm, and triangle with  $r_v$  and  $r_c$  of 2 mm. The nominal length of the longest edge is 63.2 mm.

### Appendix: Estimating the Center of Mass Locus

Variations in part shape result in uncertainty in the location of the part center of mass. Our tolerance model permits the center of mass location and its uncertainty disk radius to be specified as independent variables that are not functions of the vertex locations and uncertainty radii. We now consider the case of a polygon with uniform density whose center of mass locus depends on the vertex locations and the radii of the vertex uncertainty disks.

Consider analytically bounding the possible locations of the center of mass. To do this, triangulate the polygonal part and find the locus of center of mass locations of each constituent triangle. The center of mass of a triangle  $i$  with vertices at  $(x_{i1}, y_{i1})$ ,  $(x_{i2}, y_{i2})$ , and  $(x_{i3}, y_{i3})$  is located at

$$(x_i, y_i) = \left( \frac{x_{i1} + x_{i2} + x_{i3}}{3}, \frac{y_{i1} + y_{i2} + y_{i3}}{3} \right).$$

This implies that the locus of the center of mass of a triangle with vertex uncertainty disks of radius  $r_v$  is a disk of radius  $r_v$ . The mass of a triangle with uniform density is proportional to its area. The area of the triangle,  $A_i$ , also varies with the vertex locations and is given by

$$A_i = \frac{x_{i1}(y_{i2} - y_{i3}) + x_{i2}(y_{i3} - y_{i1}) + x_{i3}(y_{i1} - y_{i2})}{2}.$$

Let  $(x_{COM}, y_{COM})$  represent the center of the mass of the polygon and let  $(\hat{x}_{ij}, \hat{y}_{ij})$  represent the nominal location of vertex  $j$  of triangle  $i$ . Then

$$x_{COM} = \left( \sum_i x_i A_i \right) / \left( \sum_i A_i \right)$$

$$y_{COM} = \left( \sum_i y_i A_i \right) / \left( \sum_i A_i \right)$$

subject to  $(x_{ij} - \hat{x}_{ij})^2 + (y_{ij} - \hat{y}_{ij})^2 \leq r_v^2, \forall i \text{ and } j = 1, 2, 3.$

We see that the center of mass locus of an arbitrary convex polygon does not have a simple description similar to that of a triangle. Assuming the shape instantiations of the constituent triangles are independent, finding the extremal locations of the polygon center of mass amounts to finding the extreme values of its  $x$  and  $y$  coordinates, with constraints on the permitted vertex locations. We can use the smallest disk that encloses these extremal points to obtain a conservative bound on the locus of the center of mass. Finding the exact locus of the center of mass is an open problem. See Bern et al. (1995) for related work on estimating the locus of the centroid of a set of points whose weights vary within known ranges.

For convenience, we estimate center of mass variations by randomly sampling the variational class of valid part shapes. We allow each vertex to assume a random location within its uncertainty disk, determine the resulting uncertainty polygon, and compute its center of mass. By performing this random sampling over several thousand trials (100,000 in our tests), we obtain an indication of the bounds of the center of mass locus. Such sampling shows that the center of mass of a polygon with shape uncertainty can lie outside the disk of radius  $r_v$  centered at the nominal center of mass (Fig. 26). We identify the smallest circumscribing disk for the randomly sampled center of mass locations and use the disk enlarged by a safety factor as the center of mass locus of the polygon.

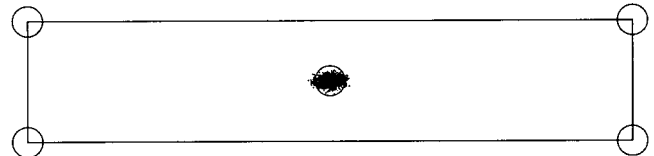


Fig. 26. A plot of the center of mass locations of 1000 randomly generated instances of a rectangle consistent with its tolerance values. This illustrates that the center of mass can lie outside a disk of radius  $r_v$ , the vertex uncertainty disk radius, at the nominal center of mass location.



## Acknowledgments

Funding was provided by NSF under grants IRI-9213993 and IRI-9318496 (with ARPA). We thank Marshall Bern, Randy Brost, Mike Erdmann, Ken Goldberg, Seth Hutchinson, and Reid Simmons for helpful suggestions and comments.

## References

- Akella, S. 1996 (December). *Robotic Manipulation for Parts Transfer and Orienting: Mechanics, Planning, and Shape Uncertainty*. Ph.D. thesis, The Robotics Institute, Carnegie Mellon University, Pittsburgh, PA. Robotics Institute Technical Report CMU-RI-TR-96-38.
- Akella, S., Huang, W. H., Lynch, K. M., and Mason, M. T. 1997. Sensorless parts orienting with a one-joint manipulator. *IEEE International Conference on Robotics and Automation*, Albuquerque, NM, April, pp. 2383–2390.
- Akella, S., and Mason, M. T. 1995. Parts orienting by push-aligning. *IEEE International Conference on Robotics and Automation*, Nagoya, Japan, May, pp. 414–420.
- Akella, S., and Mason, M. T. 1998. Parts orienting with shape uncertainty. *IEEE International Conference on Robotics and Automation*, Leuven, Belgium, May, pp. 565–572.
- Akella, S., and Mason, M. T. 1999. Using partial sensor information to orient parts. *International Journal of Robotics Research* 18(10):963–997.
- American Society of Mechanical Engineers. 1995. *Dimensioning and Tolerancing, Y14.5M-1994*, New York: Author.
- Bern, M., Eppstein, D., Guibas, L. J., Hershberger, J. E., Suri, S., and Wolter, J. 1995. The centroid of points with approximate weights. *Proc. 3rd Eur. Symp. Algorithms*, Lecture Notes in Computer Science, No. 979, pp. 460–472. New York/Berlin: Springer-Verlag.
- Brost, R. C. 1988. Automatic grasp planning in the presence of uncertainty. *International Journal of Robotics Research* 7(1):3–17.
- Brost, R. C., and Christiansen, A. D. 1996. Probabilistic analysis of manipulation tasks: A conceptual framework. *International Journal of Robotics Research* 15(1):1–23.
- Brost, R. C., and Peters, R. R. 1996. Automatic design of 3-D fixtures and assembly pallets. *IEEE International Conference on Robotics and Automation*, Minneapolis, MN, April, pp. 495–502.
- Caine, M. 1994. The design of shape interactions using motion constraints. *IEEE International Conference on Robotics and Automation*, San Diego, CA, May, pp. 366–371.
- Chen, J., Goldberg, K. Y., Overmars, M. H., Halperin, D., Bohringer, K. F., and Zhuang, Y. 1998. Shape tolerance in feeding and fixturing. In *Robotics: The Algorithmic Perspective*, ed. P. K. Agarwal, L. E. Kavraki, and M. T. Mason, 297–311. Natick, MA: A. K. Peters.
- Chen, Y.-B., and Ierardi, D. J. 1995. The complexity of oblivious plans for orienting and distinguishing polygonal parts. *Algorithmica* 14:367–397.
- Christiansen, A. D. 1992 (March). *Automatic Acquisition of Task Theories for Robotic Manipulation*. Ph.D. thesis, School of Computer Science, Carnegie Mellon University, Pittsburgh, PA. Technical Report CMU-CS-92-111.
- Deacon, G. E., Wright, M., and Malcolm, C. 1997 (September). Qualitative transitions in object reorienting behaviour, Part 2: The effects of varying the center of mass. Technical Report DAI Research Paper No. 864, Department of Artificial Intelligence, University of Edinburgh, Edinburgh, UK.
- Donald, B. R. 1989. A geometric approach to error detection and recovery for robot motion planning with uncertainty. *Artificial Intelligence* 37(1–3):223–271.
- Donald, B. R. 1990. Planning multi-step error detection and recovery strategies. *International Journal of Robotics Research* 9(1):3–60.
- Erdmann, M. 1992. Randomization in robot tasks. *International Journal of Robotics Research* 11(5):399–436.
- Erdmann, M., and Mason, M. T. 1988. An exploration of sensorless manipulation. *IEEE Journal of Robotics and Automation* 4(4):369–379.
- Goldberg, K. Y. 1993. Orienting polygonal parts without sensors. *Algorithmica* 10(2/3/4):201–225.
- Inui, M., Miura, M., and Kimura, F. 1996. Positioning conditions of parts with tolerances in an assembly. *IEEE International Conference on Robotics and Automation*, Minneapolis, MN, April, pp. 2202–2207.
- Joskowicz, L., Sacks, E., and Srinivasan, V. 1997. Kinematic tolerance analysis. *Computer-Aided Design* 29(2):147–157.
- Kavraki, L. 1997. Part orientation with programmable vector fields: Two stable equilibria for most parts. *IEEE International Conference on Robotics and Automation*, Albuquerque, NM, April, pp. 2446–2451.
- Latombe, J.-C., Wilson, R. H., and Cazals, F. 1997. Assembly sequencing with toleranced parts. *Computer-Aided Design* 29(2):159–174.
- Mason, M. T. 1986. Mechanics and planning of manipulator pushing operations. *International Journal of Robotics Research* 5(3):53–71.
- Neumann, A. G. 1994. The new ASME Y14.5M standard on dimensioning and tolerancing. *Manufacturing Review* 7(1):9–15.
- Nievergelt, J., and Preparata, F. 1982. Plane-sweep algorithms for intersecting geometric figures. *Communications of the ACM* 25(10):739–747.
- Peshkin, M. A., and Sanderson, A. C. 1988. The motion of a pushed sliding workpiece. *IEEE Journal of Robotics and Automation* 4(6):569–598.
- Preparata, F. P., and Shamos, M. I. 1985. *Computational Geometry: An Introduction*. New York/Berlin: Springer-Verlag.

- Rao, A. S., and Goldberg, K. Y. 1994. Shape from diameter: Recognizing polygonal parts with a parallel-jaw gripper. *International Journal of Robotics Research* 13(1):16–37.
- Requicha, A.A.G. 1983. Toward a theory of geometric tolerancing. *International Journal of Robotics Research* 2(4):45–60.
- Requicha, A.A.G. 1984. Representation of tolerances in solid modeling: Issues and alternative approaches. In *Solid Modeling by Computers: From Theory to Applications*, ed. M. S. Pickett and J. W. Boyse, 3–22. New York: Plenum.
- Requicha, A.A.G. 1993. Mathematical definition of tolerance specifications. *Manufacturing Review* 6(4):269–274.
- Rich, E., and Knight, K. 1991. *Artificial Intelligence*. 2d ed. New York: McGraw-Hill.
- Taylor, R. H., Mason, M. T., and Goldberg, K. Y. 1988. Sensor-based manipulation planning as a game with nature. In *Robotics Research: The Fourth International Symposium*, ed. R. C. Bolles and B. Roth, 421–429. Cambridge, MA: MIT Press.
- Voelcker, H. 1993. A current perspective on tolerancing and metrology. *Manufacturing Review* 6(4):258–268.
- Walker, R. K., and Srinivasan, V. 1994. Creation and evolution of the ASME Y14.5.1M standard. *Manufacturing Review* 7(1):16–23.
- Yap, C. K. 1995 (September). Exact computational geometry and tolerancing metrology. In *Snapshots of Computational and Discrete Geometry, Volume 3*, ed. D. Avis and J. Bose. McGill School of Computer Science Technical Report No. SOCS-94.50, Montreal, Quebec.